Ana Catarina Candeias Mota

Bachelor in Micro and Nanotechnologies Engineering Sciences

Real-time droplet monitoring for digital Polymerase Chain Reaction in microfluidic chip

Dissertation submitted in partial fulfillment
of the requirements for the degree of

Master of Science in
Micro and Nanotechnologies Engineering

Adviser: Dr. Joana Neto, Postdoctoral Research Associate, NOVA University of Lisbon
Co-adviser: Dr. Hugo Águas, Associate Professor, NOVA University of Lisbon

Examination Committee

Chair: Dr. Rodrigo Ferrão de Paiva Martins
Rapporteurs: Dr. Sara Abalde-Cela
Members: Dr. Joana Sofia Pereira Neto

FACULDADE DE CIÊNCIAS E TECNOLOGIA
UNIVERSIDADE NOVA DE LISBOA

March, 2021

Real-time droplet monitoring for digital Polymerase Chain Reaction in microfluidic chip

This document was created using the (pdf)LaTeX processor, based on the NOVAthesis template, developed at the Dep. Informática of FCT-NOVA by João M. Lourenço.

"Pedras no caminho? Guardo todas, um dia vou construir um castelo..."

- Fernando Pessoa

Acknowledgements

Em primeiro lugar queria agradecer à minha orientadora Joana e ao André por todo o conhecimento que me transmitiram ao longo destes meses. Obrigada por todas as formações, por todas as dicas, por promoverem o meu pensamento critíco e por toda a paciência. Vocês foram incríveis comigo!
Ao Professor Hugo Águas por todos os ensinamentos ao longo destes anos e ao longo destes meses de trabalho e por ter despertado a minha curiosade sobre a microfluídica.
Ao Gonçalo, por toda a ajuda prestada em relação ao Bonsai e a todos aqueles que, de uma maneira ou de outra, me ajudaram ao longo deste percurso.
À FCT por ter sido a casa que me acolheu nestes últimos 5 anos e que me fez crescer como pessoa.
À minha família porque sem eles nada disto seria possível. Mãe, o meu obrigada por tudo. Obrigada por me teres dado a oportunidade de frequentar a universidade e por nunca deixares de acreditar em mim.
À minha avó, por todas as comidinhas boas que me envia e ao meu avô por servir de chauffer sempre que precisava e ao qual tirei a veia de engenharia.
Ao meu irmão Rui por toda a paciência que tem para me aturar e ao meu irmão Carlos.
Aos restantes familiares que me acompanharam nesta jornada.
Por fim, quero agradecer ao melhor que a faculdade me deu, Daniel, obrigada meu amor por todo o apoio incondicional, por celebrares as minhas vitórias e por me puxares para cima sempre que estou mais em baixo.

Abstract

Current cancer diagnosis techniques are often dependent on the collection of tumour tissue, involving invasive processes for the patient. Circulating Tumour DNA (ctDNA) emerges as an alternative resource for cancer detection and monitoring, that can be harvested from simple blood samples. Digital Polymerase Chain Reaction (dPCR) is a fast and sensitive technique for DNA amplification, suitable for low DNA concentrations such as ctDNA. Advances in microfluidics allow the partition of PCR samples into droplets based in water-in-oil emulsions, so that PCR amplification occurs within each droplet. In this way, the PCR reaction is a well controlled process with a low probability of contamination and allowing a high throughput analysis.

The aimed of this work was to develop droplet-based microfluidic device for application to dPCR technique coupled with real-time droplet monitoring. This work focused on the design and fabrication of a microfluidic device capable of producing a large number of uniform droplets with volumes in the nanoliter range and constant frequency. For this, a polydimethylsiloxane (PDMS) droplet generator device was developed, through photo and soft-lithography techniques, and tested with several oil/water flow rates ratios. Then, the droplets generated were characterized in terms of droplet size, velocity and frequency through the implementation of a powerful open-source software for real-time analysis. Several tests on different devices were carried out to evaluate the device reproducibility. Finally, the droplet generator was incorporated with a serpentine design, allowing the PCR cycles to occur in continuous flow.

The results revealed that was possible to generate droplets with radius between 22-99 μm and a coefficient of variation bellow 10%. The correspondents volumes ranged between 90 pL-4.18 nL. Moreover, the velocities obtained situated between 0.05 mm/s-7.62 mm/s with droplet generating frequency of 2-50 Hz.

Regarding to the droplet monitoring, the results of the workflows developed revealed similarity with the results obtained trough a widely used software for this purposes, with the advantage of allowing real-time analysis for a larger sample of results.

Keywords: dPCR, Microfluidic, Droplet generator, Droplet-based microfluidic, label-free, real- time droplet monitoring;

Resumo

As técnicas actuais usadas no diagnóstico de cancro, geralmente dependem da recolha de tecido tumoral, envolvendo processos invasivos para o paciente. O DNA tumoral circulante (ctDNA) surge como alternativa para a detecção e monitorização do cancro, podendo ser extraído através de amostras de sangue. A reação em cadeia da polimerase de modo digital (dPCR) é uma técnica rápida e sensível para amplificação de DNA, adequado para baixas concentrações de DNA, como o ctDNA. Os avanços na microfluídica permitem a partição das amostras de PCR em gotas com base em emulsões de água em óleo, de modo que a amplificação por PCR ocorra dentro de cada gota. Deste modo, a reação de PCR é um processo bem controlado com baixa probabilidade de contaminação, permitindo uma análise de alto rendimento.

Este trabalho teve como objetivo o desenho e a fabricação de um dispositivo de microfluídica capaz de produzir um elevado número de gotas uniformes, cujos volumes se encontram na gama dos nanolitros, com frequência constante. Para tal, foi desenvolvido um dispositivo para geração de gotas em polidimetilsiloxano (PDMS), através de técnicas de fotolitografia e litografia suave, tendo sido testado com diversas taxas de fluxos entre óleo / água. Posteriormente, as gotas geradas foram caracterizadas em relação ao seu tamanho, velocidade e frequência através do software de análise de vídeo Bonsai. Diversos testes em diferentes dispositivos foram realizados de modo a avaliar a reprodutibilidade do dispositivo. Por último, o gerador de gotas foi incorporado com desenho da serpentina, permitindo que os ciclos de PCR ocorram em fluxo contínuo.

Os estudos realizados revelaram que foi possível gerar gotas com raios entre 22-99 μm, e coeficiente de variação inferior a 10%. Os volumes correspondentes variaram entre 90 pL-4.18 nL. Além disso, as velocidades obtidas situaram-se entre 0.05 mm/s-7.62 mm/s com frequência de geração de gotas de 2-50 Hz.

Relativamente à monitorização das gotas, os resultados dos workflows desenvolvidos revelaram similaridade com os resultados obtidos através de um software amplamente utilizado para estes fins, com a vantagem de permitir a análise em tempo real para uma amostra maior de resultados.

Palavras-chave: dPCR, Microfluidica, Gerador de Gotas, Microfluidica baseada em gotas, Monitorização em tempo real das gotas

Contents

List of Figures

List of Tables

Acronyms

BGR	Blue, Green, Red
ctDNA	Circulation Tumour DNA
CV	Coefficient of Variation
DNA	Deoxyribonucleic Acid
dPCR	Digital Polymerise Chain Reaction
DWL	Direct Write Laser
IPA	Isopropyl Alcohol
LOC	Lab-on-chip
MQ	Deionized Water
PCR	Polymerase Chain Reaction
PDMS	Polydimethylsiloxane
ROI	Region of Interest
UV	Ultra Violet Electromagnetic Radiation
WHO	World Health Organization

Chapter One

Motivation and Objectives

Cancer is one of the leading causes of death in the world, causing millions of deaths each year. World Health Organization (WHO) estimates that in 2030 it will be between 10 to 11 million newly diagnosed cases and the number of deaths can reach over 13 million [1]. The mortality rate associated with this disease can be reduced through its early detection and monitoring [2].

In this way, liquid biopsy emerges as a fast, non-invasive technique for cancer diagnosis and its monitoring through the blood sample collection. Circulating tumor DNA (ctDNA), present in bloodstream, can provide real-time information about the current status of the disease. Digital PCR (Digital Polymerase Chain Reaction) is a sensitive and precise technique for detection of rare ctDNA present in bloodstream, that allows the partition of PCR sample into small volumes, such as droplets, leading PCR amplification to occur within each droplet.

The aim of this work was to develop a microfluidic device able for droplet-based DNA amplification. To achieve this goal, several objectives needed to be met as follows:

- Fabrication through photo and soft-lithography techniques of a high-throughput droplet-based microfluidics generator;
- Real-time optimization and characterization of droplet parameters in terms of size, velocity and frequency through the use of a powerful open-source software;
- Integration of droplet-based continuous-flow microfluidic PCR, optimizing flow rates according to droplet residence time for each phase of PCR cycle.

Chapter Two

Introduction

2.1 Circulating Tumour DNA

Current cancer diagnosis techniques generally involves collection of tumour tissue which require invasive surgeries or biopsies.
Liquid biopsy emerges as a faster and non-invasive method for collection of cancer biomarkers, such as circulating tumour DNA (ctDNA). The ctDNA is DNA fragments in the bloodstream originated from tumors and cancerous cells, which allows early cancer detection and provides instant information about the status of the patient and response to the therapy prediction [3–5]. However, ctDNA concentration in bloodstream can be extremely low, whereby its detection requires a high sensitive technique [6].

2.2 Polymerase Chain Reaction (PCR)

Polymerase Chain Reaction (PCR) is a widely used technique for DNA amplification, allowing the exponentially generation of copies of a specific DNA target. Its principle consists in submitting the sample between three thermal-cycling processes: denaturation of double-strand DNA, annealing of primers and primer extension [7].

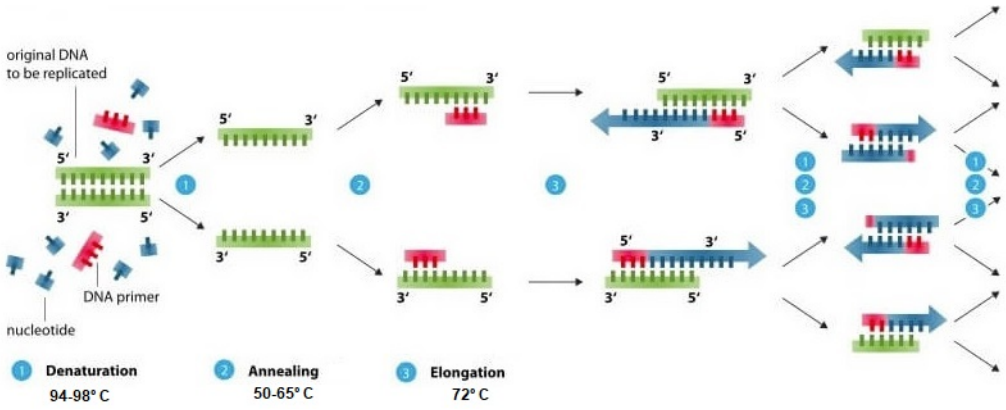

Figure 2.1: Schematic of PCR process: [8]

During denaturation phase, the sample is heated to temperatures between 94-98° C that allows the separation of DNA single strands, opening the path for primers, nucleic acid segments necessary to initiate DNA amplification. Then, the annealing phase is carried out at 50-65° C, allowing the primers to bind to the target DNA sequence and initialize the polymerization process, i.e., the formation of new DNA strand from free nucleotide. Lastly, at extension phase at 72° C, new strand of DNA are formed using the original strands as templates [7, 8]. Once one cycle of PCR is completed, two double-stranded sequences of target DNA are formed, being one of the strands new and the other one being the original strand [8, 9]. Repeating this process for 20-30 cycles, it is possible to

amplify the DNA in up to 100000 copies [7, 10].
However, PCR estimates the amount of amplified products at the end of cycles, comparing the results with a known standard curve [10–13], resulting in qualitative results with low sensitivity, resolution and precision.

2.3 Digital Polymerase Chain Reaction (dPCR)

To overcome the qualitative results associated to traditional PCR, digital Polymerase Chain Reaction (dPCR) emerges as a fast and sensitive technique that allows quantitative information about the amount of nucleate acids formed during amplification process [12].

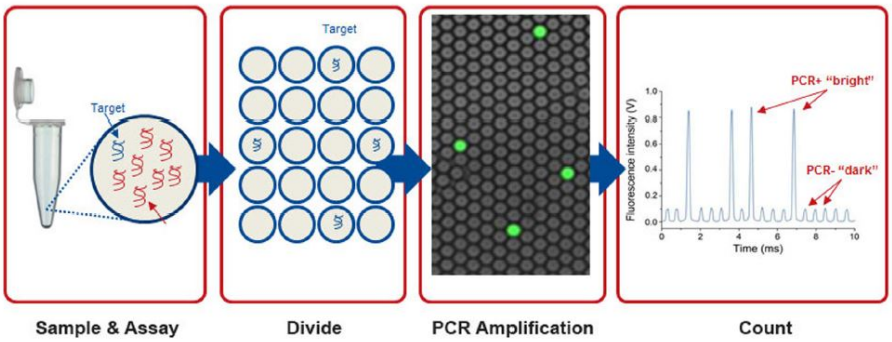

Figure 2.2: Schematic of dPCR process: sample partition and digital counting for quantitative results [14]

The breakthrough of this technique consists in the partition of PCR sample into thousands of small portions with few nanoliters of volume that will function as individual and parallel PCR reactors, such as droplets. The name dPCR is related to the presence or abstinence of the target DNA molecule inside each reactor, that will show a positive (1) or negative (0) signal during amplification [15].
After PCR amplification, reactors that contain the target sequence, i.e, positive cases, emit fluorescence signals, contrary to negative cases. Thus, the fraction of negative cases is used to generate an absolute count of the number of target molecules present in the sample. Poisson distribution is used as a correction factor for the cases that, although rare due to PCR sample dilution, one droplet contains more than one molecule per reaction [12, 13, 16]. In this way, it is possible to have an absolute quantification about the number of nucleotides formed during the amplification process, without the need to resort to standard controls as in the case of traditional PCR.
Since dPCR reactors are evaluated individually, the results are not affected by variations in amplification efficiency as well as the signal-to-noise ratio increases due to the reduction of background signal leading to an increase in detection sensitivity. [16, 17]

2.4 Microfluidics

Microfluidics (μFL) emerged as a field related to the behavior and precise manipulation of fluids at a micrometer scale inside channels, whose size can range from ten to hundreds of microns. This concept allowed the miniaturization of several laboratory process leading to Lab-on-chip (LOC) concept [18]
Microfluidic devices offers several advantages over conventional chemical and biological methods. Some advantages that can be highlighted are the small volume of sample and reagents needed, since microfluidics is able to handle volumes between 10^{-9}-10^{-18} L. As a result, sample loss is prevented and sample dilution is decreased leading to high resolution and sensitivity detection. Moreover, it is possible to undergo analysis with limited sample as well as handling costly and/or hazardous reagents. [19, 20]
The small sizes associate with these type of structures results in faster reaction times, temperature control, portability and low costs of production [18].
During the early 21st century, microfluidics became a versatile tool at different fields, having extended its concept to areas such as paper-based devices, organ-on-chip devices and droplet-based PCR, the latter being the focus of this work.
Microfluidic devices can be made with different materials according to the application. Among these, silicon, glass and polymers are contenders. Concerning silicon, it has the great advantage of existing a well-development processes due to semiconductor industry and, thus, allowing complex structures. Additionally, it has a high thermal conductivity that allows fast PCR cycles. However, its opacity limits the detection process. Despite glass overcomes the problem of silicon opacity, it has high fabrication costs and long processing times. In this way, polymers emerges as a material that can overcome the described problems. Within them is the PDMS, which has the advantages of having a low cost, high flexibility, transparency to allow optical and bio-compatibility [21, 22].

2.5 Droplet Formation

The combination of droplets with microfluidics is a promising technological development for novel microfluidic devices that allows chemical and biological fast analysis, reducing the sample consumption due do the small volumes required [23].
The principle of droplet generation is based on emulsions formations through immiscible phases. Typically, these phases are constitute by an organic fluid, such as oil, and an aqueous fluid that, due to their different viscosities, avoid to interact each other. Thus, water phase is broken by oil phase, generation droplets. [24–27]
The most common geometry for droplet generation is the flow-focusing devices (Fig: 2.3) with a junction that represents the intersection between three or more channels [25, 27]. Disperse phase, that will be encapsulated into droplets, is broken-up by continuous phase, in which droplets will be encapsulated, generating droplets with high monodispersity and high formation frequencies.

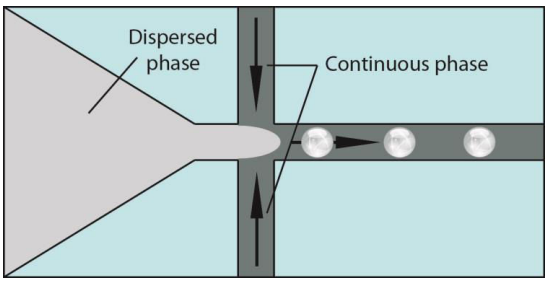

Figure 2.3: Scheme of Flow Focusing geometry for droplet generation [28]

By controlling the flow rate of disperse and continuous phase, and the width of junction, it is possible to produce high monodisperse droplets with controllable size, velocity and frequency [24, 27, 29, 30]. Current studies demonstrate droplet with a formation frequency up to 10000 Hz (1000 droplets per second) with a variation coefficient of droplet diameter less than 2% [24]. Due to high control of droplets features, flow-focusing geometry will be used for this work.
Surfactants, surface active agent, are added to continuous phase, playing an important role concerning droplet stability, guaranteeing the non-coalescence of droplets. The main purpose of surfactants is to decrease the surface and interfacial tension and stabilize the interface [31].
One of the great advantages of droplet is that it offers a perfect isolated environmental, functioning as individual reactors that allows process control and a high-throughput observation of its chemical and biological interactions among large population. Therefore, we will then discuss the most important and exciting recent developments in continuous-flow microfluidic PCR in droplets with on-chip thermocycling.

2.6 Droplet Monitoring Techniques

Several techniques allow real-time monitoring of droplet parameters and their contents. However, most of these techniques involve fluorescence-labeling which, despite being effective for droplet content evaluation, their use can affect the chemical and biological behavior of the content and thus compromise clinical application [32].
Several techniques have been developed to overcome the problem of detection based on fluorescence labeling, such as offline video analysis software [33], intensity measurements through photodiodes triggered by the camera [21], impedimetric measurements in real-time [34] and optoacoustic-fluidic microscopy [35]. However, those techniques involve high complexity, becoming time-consuming for the user with high costs and low detection rates associated [32].
To overcome the problems described, Bonsai emerges as an open-source software that allows the analysis and monitoring of droplets in real-time, as well as obtaining information about their contents not relying on fluorescent-labeling.

2.7 Bonsai: Open-Source Software

To overcome the challenges presented by the techniques described in section 2.6, it is proposed the utilization of Bonsai. Besides, nowadays most scientific experiments require the control and monitoring of many parallel data streams that comes from different hardware, each one associated with their own software. As a result, the user needs in-sights for each one, which implies a significant amount of time spent for setting up experiments. In order to face these obstacles, Bonsai emerges as open-source and high-performance software that allows a fast analysis of several parallel data streams in real-time through a visual language, suitable for software systems that require rapid and detailed interaction with the experiments. [36]. In addition, it is also possible to implement methods for real-time analysis and active hardware (e.g., syringe pumps) manipulation using a closed loop workflow.
Regarding dPCR in continuous flow, the velocity through the isothermal regions need a stable velocity. Therefore, Bonsai has the possibility to adjust the flow rates to adapted these velocities. In this way, Bonsai emerges as powerful tool for droplet monitoring and for the real-time interaction between droplets and its setup.

2.7.1 Working principle

In Bonsai, interactive systems can be represented by reactive networks constituted by nodes interconnected according to data propagation. The workflow where these nodes are inserted represents a sequence of observable events that need to be completed sequentially or in parallel until achieving the desired output, with a capacity of visualizing the state of data at different stages [37]. Figure: 2.4 represents different types of nodes existent for observable sequences.

Category	Description	Category	Description
Source	generate event streams from devices or files	Sink	save data or trigger external outputs
Transform	convert or process individual data items	Combinator	manage control flow or synchronize parallel inputs
Condition	filter data items matching some specific condition		

Figure 2.4: Bonsai: Different type of nodes for creating observable sequences [37]

Chapter Three

Materials and Methods

All chemicals were purchased at Sigma-Aldrich unless otherwise specifically stated.

3.1 Microfluidic Device Fabrication

The microfluidic devices were made using polydimethylsiloxane (PDMS). The hard mask was produced by using Direct Write Laser (DWL), the design of which was made previously at AutoDesk® AutoCAD.

3.1.1 Hard-mask fabrication

In a clean glass substrate, Molybdenium was deposited through sputtering (50 sscm of Argon flow, 1.7 mTorr at 175 W). A positive photorresist (AZE CI3012, MicroChemicals GmbH) was spun-coated on top of the glass and the patterning was carried out at DWL. Afterwards, the sample was immersed in a container with developer (AZ726 MIF) for 30 s. Once the pattern is visible, the sample is immersed in a container with water to stop the reaction and then in another container with water to remove any photorresist residuals. Once the development process is completed, the metal is etched at dry etching system (10 sccm of SF6 flow, 50 mTorr, 60 W for 600 s). Finally, the sample is immersed in acetone and placed on a rotating table.

3.1.2 SU-8 mould fabrication

One of the most critical steps in microfluidic device fabrication is SU-8 mould fabrication. PDMS replicates all the features existing in the master mould, whereby any mould defects will affect PDMS structure. Additionaly, SU-8 2050 (MicroChem) is a viscous photoresist which properties are greatly influenced by room temperature. (Annex:I) Therefore, the spin-coating parameters have to be adjusted according to aimed thickness, batch, and room temperature.

3.1.2.1 Cleaning process

The master mould was produced on a silicon wafer substrates since it has a better adhesion to the polymer than glass and has less surface rugosity. The silicon wafer cleaning process is the same as described in section 3.1.1.

3.1.2.2 Spin Coating

SU-8 2050 (Microchem) was poured on top of the wafer (photoresist should be poured from close proximity to prevent air bubbles formation), and spin coated for 7 s at 500 rpm in order to spread the photoresist. Afterward, it was spin coated for 30 s at 1200 rpm in

order to achieve the layer thickness of 130 μm at the room temperature of 21.5º C.
The wafer was removed from the glass and let to rest for 10 min on a leveled area.

3.1.2.3 Soft-bake

The wafer was placed in a levelled hot plate for 5 min at 65º C and then for 24 min at 95º C, in order to evaporate the solvents in photoresist. Then, it was rest to cool down for about 10 min in order to avoid misalignment by thermal expansion during next step.

3.1.2.4 Exposure

The exposure of SU-8 was done using mask aligner. Since SU-8 absorbs light of wavelength below 350 nm, which can result in a T-shaped profile, the exposure was done through an i-line filter that cuts off the wavelength light below 350 nm, allowing a profile with vertical side walls. Once the filter was inserted, the light intensity was measured using an optometer to optimize exposure time. In this way, the dose used was 248.6 mJ/cm^2 for 39.8 s at constant power. The time exposure was dependent of aimed thickness and ligth intensity.

3.1.2.5 Post-bake

A post exposure baking was done at 65º C for 5 min and at 95º C for 11 min. Afterward, it was let to cool down to room temperature.

3.1.2.6 Development

This step consists of removing the unwanted SU-8 from the wafer. For that, the wafer was immersed in a container with SU-8 developer (propylene glycol monomethyl ether acetate (PGMEA)) and placed on a rotating table at around 50 rpm for 14 min. Afterward, the wafer was immersed in IPA, to stop the reaction, and rinsed with deionized water. If through an optical microscope inspection were noticed visible leftovers os SU-8, the wafer was rinsed sequentially with developer, IPA and deionized water.
Then, the wafer was placed in a hot plate at 150º C for 30 min for hard baking process.

3.1.3 PDMS chip fabrication by soft-lithography

The master mould was placed in a vacuum desiccator along with a droplet of silane (Trichloro(1H,1H,2H,2H-perfluorooctyl)silane) for 1 h which is an anti-sticking agent that facilitates the PDMS peeling off from the master mould.
PDMS replicas were prepared by mixing PDMS (Sylgard 184, Dow Corning, Spain) and curing agent in a 10:1 ratio (about 30 g per wafer). The mixture was degassed in a vacuum desiccator for about 1 h. Then, it was poured over the master mould and degassed until all the air bubbles were removed. Replicas were cured in a oven at 65º C for about 2 h

and let to rest during the night.
PDMS replicas were peeled off from mould and holes for tube connection were punched.

3.1.4 Sealing Process

Glass substrates were cut and cleaned with the same process described in 3.1.1. Afterwards, glass substrates and PDMS replicas were bounded after an oxygen plasma treatment (Zepto Low-pressure plasma systems Diener Plasma Surface Technology). The parameters used a pressure of 0.5 mbar and a power of 25 W for 60 s.
The device was placed in a hot plate as 120 ºC for 5 min with some weight added on top in order to help the sealing process.

3.2 Droplet Generator Characterization

Water-in-oil droplets were generated in a flow-focusing junction of the microfluidic device. Regarding continuous phase, 1 mL of mineral oil was mixed and vortexed with 5 μL of SPAN 80 surfactant, resulting in a surfactant concentration of 0.05 wt%. MQ-water was used as fluid for disperse phase.
Continuous and disperse phase were injected through syringes pumps (KDS Scientific Legato^{TM}) into the inlets of the device. To guarantee the absence of air in the water inlet, the oil tube was connected to the device, and oil was pushed until the water inlet was full. Afterwards, the water tube was connected and the droplet generation process started.
It is important to highlight that it is necessary to avoid air presence inside syringes and tubes in order to avoid air bubbles inside the device. Additionally, if an obstruction is detected inside channels, IPA must be injected through the inlets using a manual syringe and then removed with nitrogen jet.
The setup used for droplet monitoring consisted of a home-made LED light set placed under the device and a high-speed camera (PointGrey) placed above the device with a maximum frame rate of 150 fps and 1280 x 1024 resolution. FlyCapture® Software Development Kit (Flyr Sistems, EUA) allowed the interface between camera and computer through an USB connection, and Bonsai software was used to record the videos.
During the tests, to decrease the influence of the pressure caused by larger flows within the device, the flows of the continuous and disperse phases were gradually increased.

Chapter Four

Results and Discussion

4.1 Droplet Generator

One of the milestones of this work was the optimization of the droplet generator. For dPCR analysis, each droplet volume must be reduced to picoliter-nanoliter scale. Hence, the droplet generator must be characterized and optimized taking into account, droplet size, velocity and frequency in production.

4.1.1 Droplet Generator Design

In order to optimize the droplet generator design and minimize the costs of making several masks and devices for each design, some simulations were done through COMSOL Multiphysics®, a finite element numerical simulator that allows a fast way to model and optimize the device structure. These simulations resulted from a simulation study done previously in the scope of the project where this master thesis is inserted. Several dimensions were tested in relation to the width of the oil channel, the opening angle between the water inlet and the junction, and the width of the channel at the exit of the junction. The most promising results for the droplet generation were those described in Figure: 4.1,4.2.

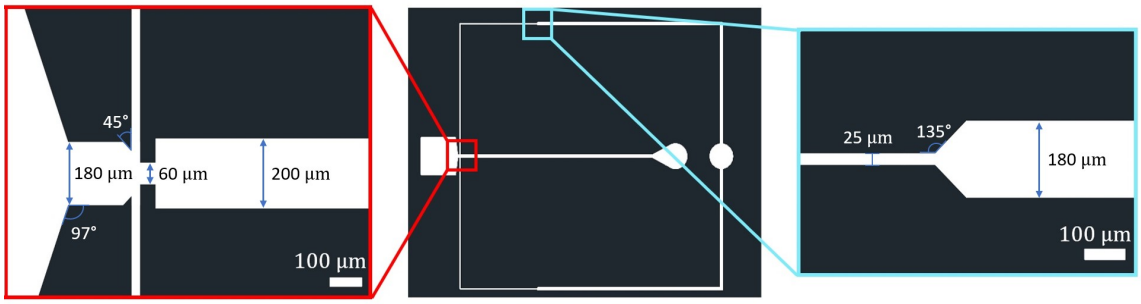

Figure 4.1: Droplet Generator Design Layout: junction Zoom (left); Oil channel (right)

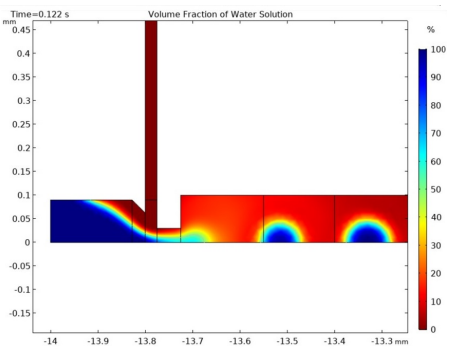

Figure 4.2: COMSOL simulations for droplet generator design: Oil flow rate at 5μL/min and Water flow rate at 2μL/min.

4.1.2 Droplet Generator Fabrication

4.1.2.1 Hard-Mask Fabrication

Initially, the patterning was done through the direct exposure of the wafer, with a layer of SU-8, in the DWL. However, aimed thicknesses greater than 100 µm requires the use of SU-8 2050 that has greater viscosity when compared to other batches able for lower thicknesses. As mentioned above, slight variations in room temperature during spin-coating process, will affect SU-8 final thickness in such way that for every 1ºC of temperature difference will result in 10 μm (Annex: I) of difference between aimed thickness according datasheet and real thickness. It was observed that the quality of the mould relies on the optimization of DWL power with SU-8 thickness.
Due to the issue that has been described, the solution found was to used DWL for designing the hard mask made of molibdenium instead of applying to Su8. Subsequently, the hard mask was used to pattern the wafer, through UV exposure in mask aligner, which is a more robust alternative process to the SU-8 2050 thickness variations.

4.1.3 Droplet Generator Device Characterization

4.1.3.1 Hard Mask

The hard mask was characterized through the optical microscope. When compared to design dimensions, the mask shows a small increase in its dimensions by approximately 3 μm on average in all directions, corresponding to an error of only 1.5 %.

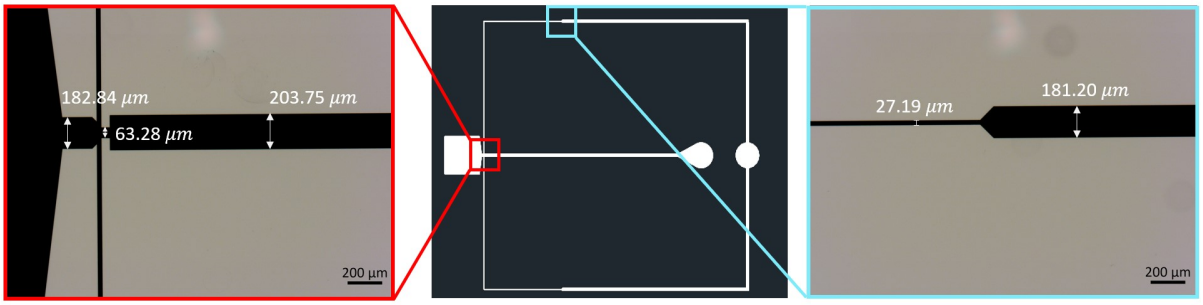

Figure 4.3: Hard Mask dimensions A) Zoom-in of the droplet generator flow-focusing junction hard mask region; B) Layout of droplet generator; C) Zoom-in of the oil channel hard mask region.

4.1.3.2 Master Mould

The protocol described in section 3.1.2.2 was conceived in order to obtain a channel height of 130 μm. Profilometer (XP-200 Ambios Technology, Inc., Santa Cruz, USA) was used to evaluate the SU-8 profile of master mould.
To evaluate thickness uniformity, profilometer measurements were made in different regions of the wafer. The results revealed thickness variation along wafer ranging from 119.56-122.95 μm which represents an average thickness of 121.55 ± 1.77 μm. Although the results showed the existence of uniformity along the wafer, there was a reduction in relation to expected thickness which can be justified by a diminution of SU-8 viscosity due to a slight increase in room temperature during spin-coating process.
Despite perfilometer being one of the most common techniques to measure feature's height, for thicknesses over 100 μm the stylus force is fixed at 10 mg which can scratch the mould.

4.1.3.3 PDMS Device

Complementary to profilometer measures, the channel height was also characterized through the device cross-section using the optical microscope. For that, a layer of PDMS was made using the process described in section 3.1.3, and poured over master mould. After curing process, the thin layer was peeled off, cut perpendicularly to the channels and inspected under the optical microscope (Figure: 3.1.3).
The results showed an increase of approximately 3 μm relatively to channel height in master mould. Additionally, the angle between the side wall and the bottom of the channel is nearly 90º C.

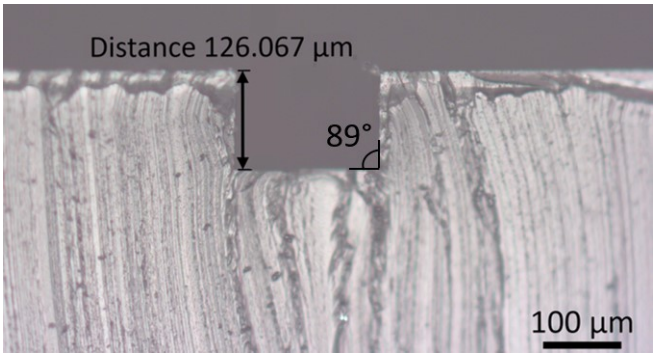

Figure 4.4: Determination of channel heigh using optical microscopy: PDMS immobilized perpendicularly under microscope depicting channel height and the perpendicularity of its sidewall.

4.2 Bonsai: Software for Droplet Characterization

Bonsai software was used for droplet size, velocity and frequency characterizations.
In Figure 4.5 is represented a scheme of setup used for droplet monitoring through Bonsai. The setup is composed by a LED light source with adjustable light controller, two microfluidic flow controllers and a high-speed camera (150 fps and 1280×1024 resolution) connected to computer by USB 3.0 cable where Bonsai is installed. The real setup is present in Annex II.

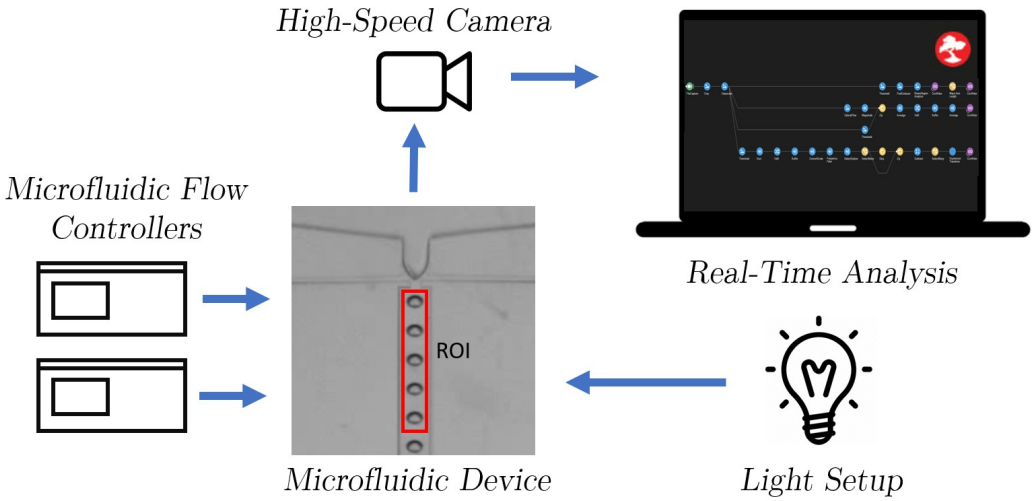

Figure 4.5: Real-Time droplet analysis setup scheme

Firstly, regarding droplet size analysis, a region of interest (ROI) must be delimited. After this, the workflow (Fig: 4.6) is set to convert the BGR image into grayscale, so that a threshold can be applied to create a binary image depending on the pixel intensity. Afterwards, it finds the contours of the image and calculates the average diameter, in pixels, through *Major Axis Length* of the droplets per frame. The results are saved in an Csv file for further analysis.

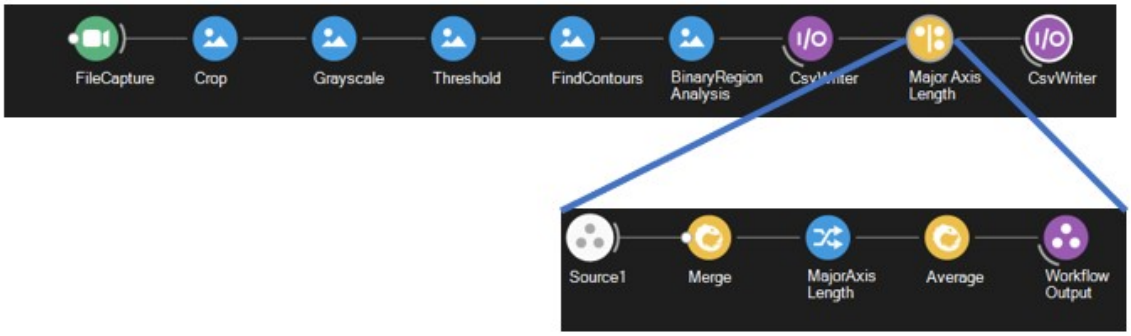

Figure 4.6: Bonsai workflow for droplet diameter calculation.

Concerning droplet velocity, the workflow (Fig: 4.7) once again starts by converting the BGR image into grayscale. Afterwards, it computes a dense optical flow through Gunnar

Farnerback's algorithm, that detects the pixel intensity between two consecutive frames giving the flow vectors of all pixels. This flow data is then used to calculate the magnitude of the mentioned vectors. Parallel to this, the workflow creates a binary image using the same Threshold node as before, which is then crossed with the flow vector magnitudes to give us the displacement of each pixel of interest.
Buffer node counts a fixed number of elements and calculates its displacement average through magnitude vector. Once again, the results are saved in an Csv file for further analysis.

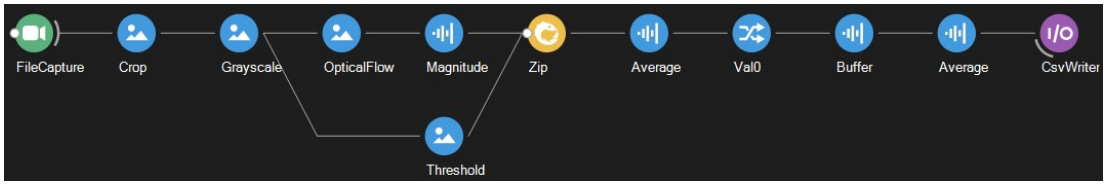

Figure 4.7: Bonsai workflow for droplet velocity calculation.

The workflow used for frequency is similar to the droplet size workflow until the *Threshold* node. Then, this workflow adds the intensity of all the pixels. A frequency filter was used to low pass the data according to the spike frequency of interest. Afterwards, *DetectSpikes* computes the time where data crossed a specific threshold, and all the spike intervals across time are merged by *SelectMany* node. Through *Subtract* node it is possible to determine the time difference between spike times. Finally, *ExpressionTransform* computes the sampling frequency trough frame rate.

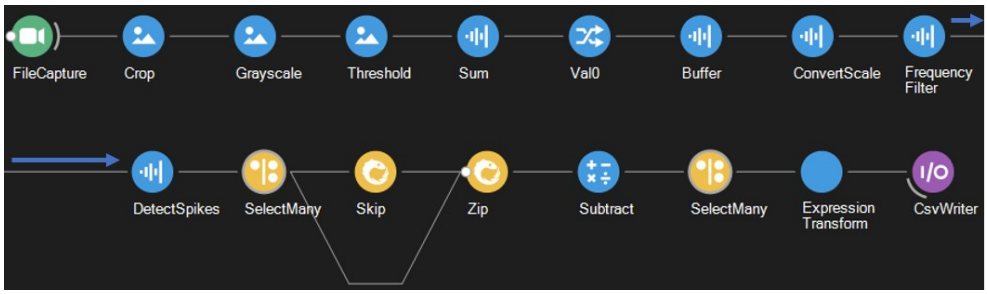

Figure 4.8: Bonsai workflow for determination of droplet generation frequency.

4.3 Bonsai Validation

All the tests were done using mineral oil with 0.05 wt% of Span-80 as continuous phase and water as dispersed phase, unless otherwise specifically stated.
To validate the use of Bonsai for droplet monitoring, the size of the droplets obtained through experimental processes were analyzed using Bonsai (Figure: 4.9) and Image J (Figure: 4.10), a widely used software for these purposes [38, 39].
Regarding droplet size calculation through Bonsai (Figure: 4.9), the workflow used is explained in section 4.2. Since the width of channel is known through the device characterization, its correspondence in pixels that can be extracted from *File Capture* node. Therefore, it is possible to calculate the micrometer per pixel ratio and thus converting the diameter obtained from Bonsai to micrometer dimension.

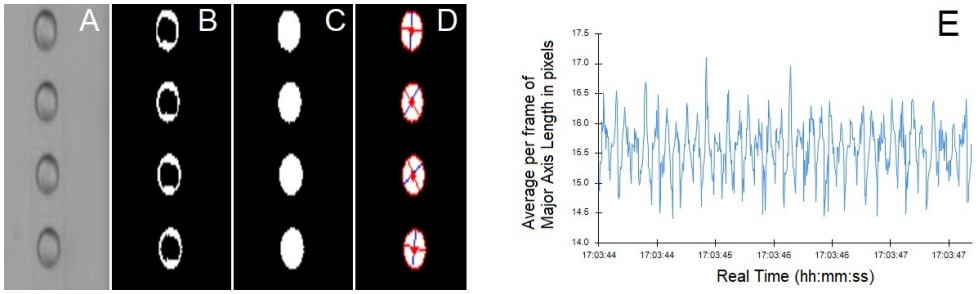

Figure 4.9: Bonsai software outputs: A) Video crop section; B) Applied threshold; C) Find Contours node output; D) Binary Region Analysis node output; E) Graphic representation of the average major axis length (represented by the red arrow in D) per frame acquisition.

Relative to Image J video analysis (Figure: 4.10), the video was imported and all frames converted into binary images, allowing the threshold process. The ROI was delimited and threshold was adjusted in such a way that all the droplet contours were defined. The scale was calibrated and through particle analysis command from Image J, and the area of each droplet situated in ROI was calculated.

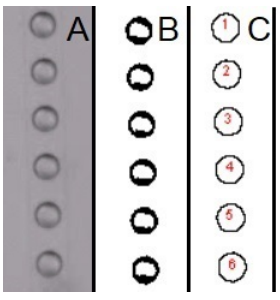

D

	Area	Mean	Min	Max
1	10560	255	255	255
2	9984	255	255	255
3	9984	255	255	255
4	10240	255	255	255
5	10176	255	255	255
6	10624	255	255	255

Figure 4.10: Image J software outputs: A) Video crop section; B) Applied threshold; C) Droplet outlines; D) Values obtained for the area associated with each droplet outline.

Fig 4.11 represents the results of the droplet radius average acquired by both software. The results revealed that there is a proximity between the radius measured by Bonsai and Image J, verifying the same trend.

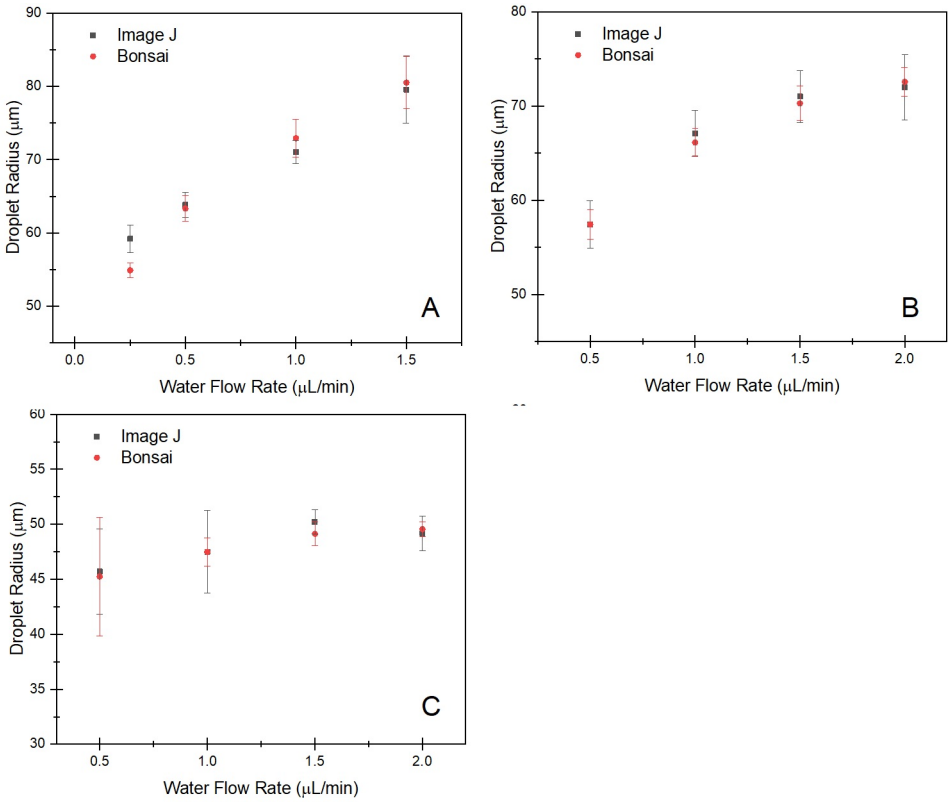

Figure 4.11: Comparison between the droplet radius measurements obtained using Bonsai and Image J, with associated standard deviation. A) Oil flow rate of 1.25 μL/min; B) Oil flow rate of 2.5 μL/min; C) Oil Flow rate of 5 μL/min.

Similar to droplet size, the Bonsai validation for the droplet velocity was also made, comparing the results obtained with Image J (Fig: 4.12).

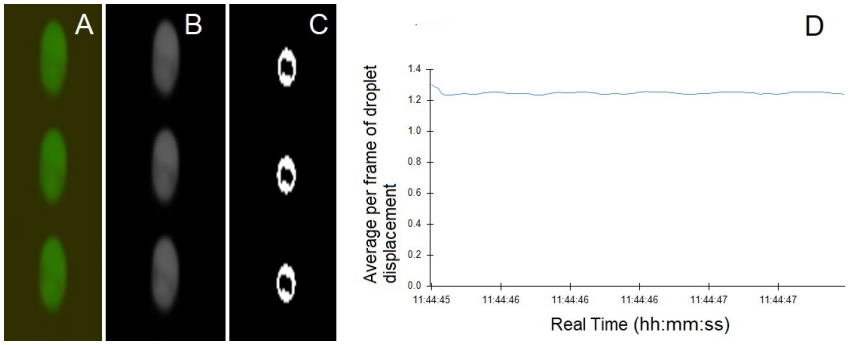

Figure 4.12: Bonsai droplet velocity workflow outputs: A) Dense Optical Flow; B) Magnitude of vectors from optical flow; C) Applied Threshold; D) Graphic representation of the average displacement of pixels per frame.

The green color represented in Fig: 4.12-A) is relative to the detection of motion in y-axis which corresponds to the direction of movement of the droplets along the channel. In the case of being any vibrations during video recording, the output of this node additionally shows the red color related to motion in x-axis.

Regarding Image J velocity analysis, wrMTrck plugin [40] was used to obtain the average droplet velocity for each video (Figure: 4.13). This procedure is similar to droplet size analysis until threshold step. Then, the plugin was started and the maximum and minimum size of features to detect were adjusted, as well as the maximum expected velocity. The results are displayed in a table where it is possible to extract information regarding average droplet speed.

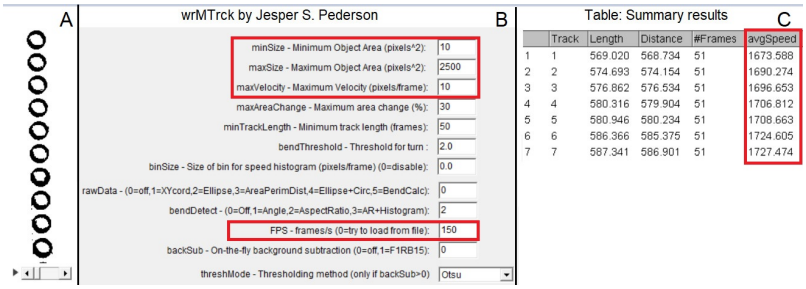

Figure 4.13: Determination of droplet velocity using Image J: A) Applied threshold for the ROI; B) Parameters configuration for droplet velocity calculation through wrMTrck plugin. Red boxes indicate the parameters to adjust for each video; C) Summary of results.

Figure: 4.14 depicts the velocity obtained through both softwares.

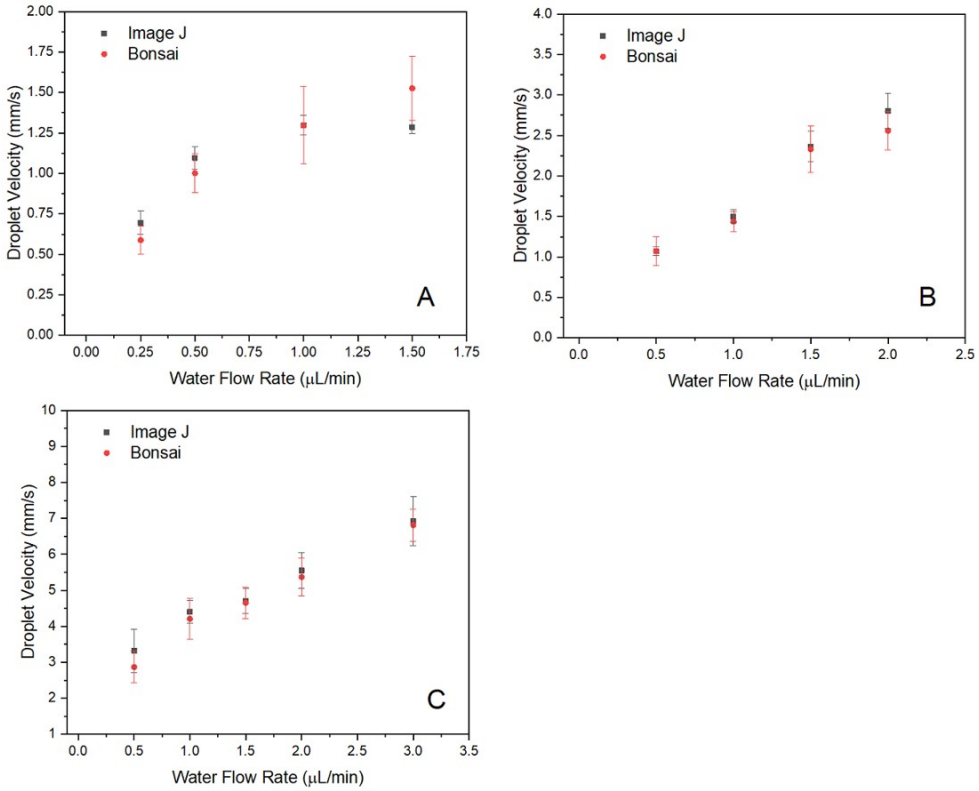

Figure 4.14: Comparison between the droplet velocity measurements obtained using Bonsai and Image J, with associated standard deviation: A) Oil flow rate of 1.25 μL/min; B) Oil flow rate of 2.5 μL/min; C) Oil Flow rate of 5 μL/min.

Once again, it is verified a proximity between Bonsai and Image J measurements. Furthermore, the results acquired from Bonsai revealed a much lower standard deviation when compared to Image J through the use of *Buffer* node that filters the environmental vibration spikes, with the advantage of allowing a faster analysis of a larger sample of results.

Regarding droplet frequency, the workflow validation was done through the comparison of the results from Bonsai to the results measured by video analysis. The latter consisted on the difference in the count of pixels between the beginning of the droplet generation at the junction and the droplet being completely formed. Through the frame rate of video it was possible to determine droplet generation frequency.

The results revealed that this workflow is suitable for droplet frequency characterization since the results are similar with those who where made manually. However, it is possible to improve this workflow to be less sensitive to the variation of its parameters, leading to smaller standard deviations.

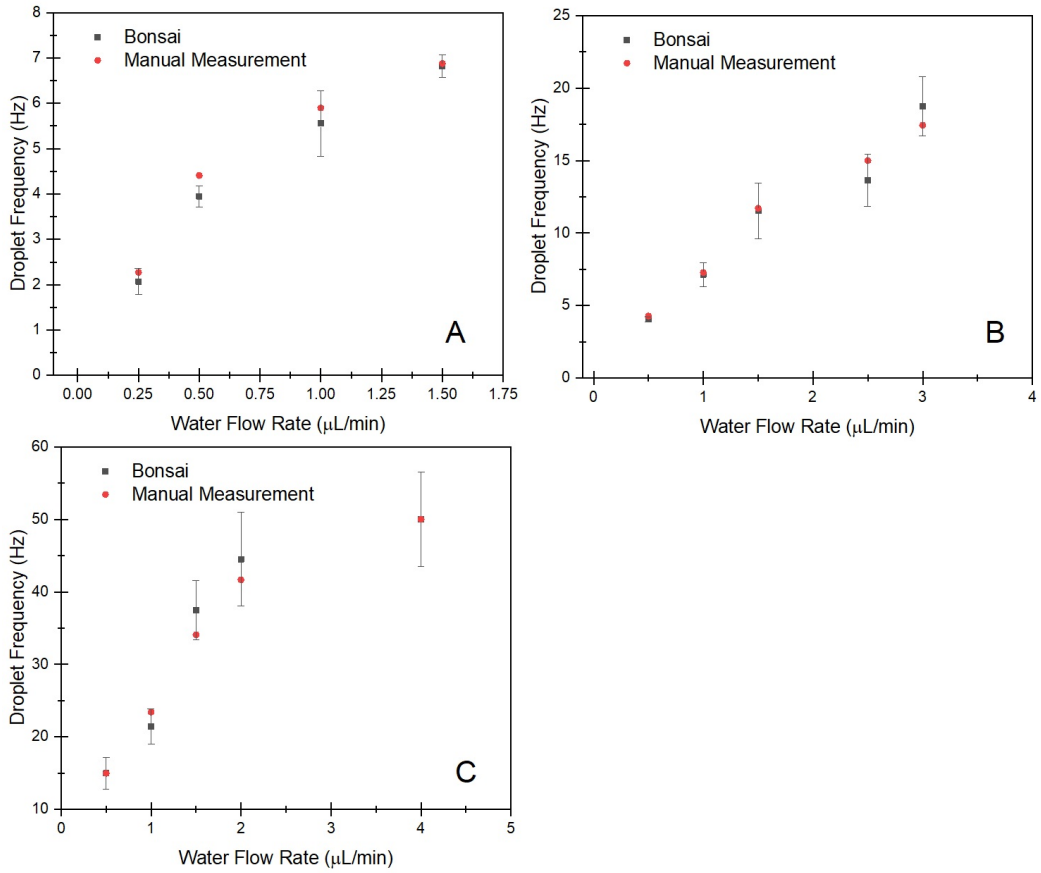

Figure 4.15: Comparison between the droplet frequency measurements obtained using Bonsai and by manual counting, with associated standard deviation: A) Oil flow rate of 1.25 μL/min; B) Oil flow rate of 2.5 μL/min; C) Oil Flow rate of 5 μL/min.

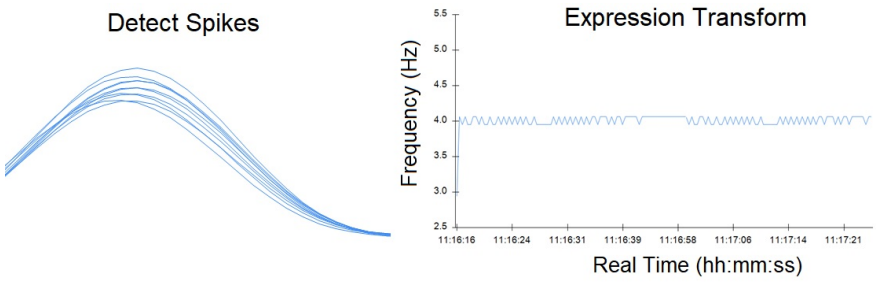

Figure 4.16: Bonsai frequency workflow output: Detect Spikes (left); Graphic representation of droplet frequency (right).

4.4 Droplet-based microfluidics generator characterization

As discussed in several articles, there are many factors that influence the size and velocity of droplets. Among these are the flow rate of disperse and continuous phase, with continuous phase having a greater influence, the viscosity of the continuous phase, and the geometry of the device [29, 41, 42].

4.4.1 Viscosity of continuous phase

To ascertain continuous phase influence, the droplets were characterized by the use of Mineral with 0.05 wt% of Span-80 concentration and Bio-rad oil (composed by Novec oil with surfactants), the latter being widely used for dPCR purposes.
Bio-rad is a global company focused on the development and fabrication of products for scientific research and clinical diagnostics. This company has commercial equipment for dPCR in which droplet emulsions are made through the use of Bio-rad oil [43]. However, this oil has a high cost. As alternative, mineral oil has lower costs and is suitable for use as an overlay to control evaporation, required for submiting droplets to temperatures closed to water boiling point, such as denaturation phase of PCR that occurs at approximately 95 ºC. It also prevents the cross contamination of samples and the droplet coalescence in emulsification systems [21].
Figure 4.17 represents the differences in droplet size (right) and velocity (left) for Mineral and Bio-rad oil used as continuous phase.
Note that the graphs for experimental data used isolated points so the lines are merely illustrative to help visualize the trend of each one. Only the nodes represent actual data points.

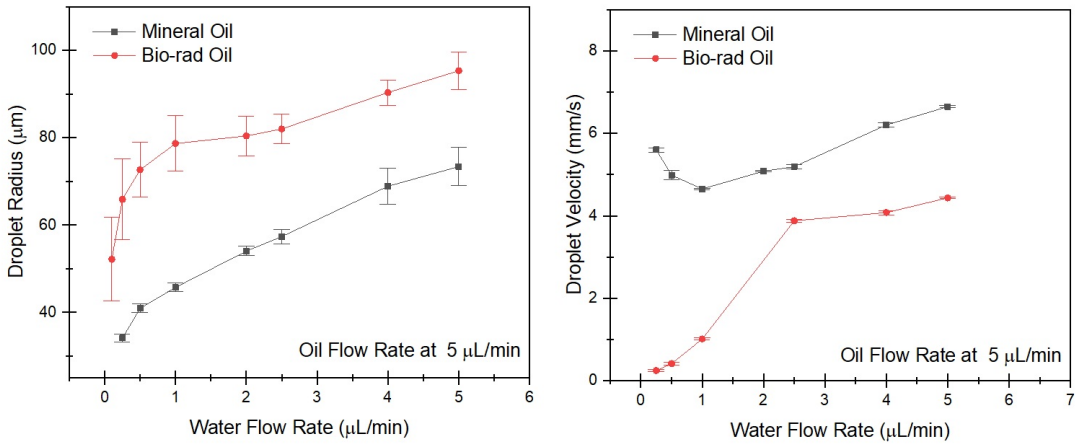

Figure 4.17: Comparison between droplet radius (left) and velocity (right) obtained for Mineral and Bio-rad oil.

Due to the low-flow rates, the droplets will be probably transported closer to the channel wall. As a result, they will move more slowly than the oil in the center of the channel. In this case, the buoyancy force is larger than the lift force [23]. A water droplet immersed in an oil carrier-fluid will experience a force due to buoyancy, which is proportional to the density difference between the droplet and the carrier-fluid. The Bio-rad oil has a density of 1.6 g/cm^3, Mineral oil with Span-80 has a density of 0.84 g/cm^3 and the water has a density of 0.99 g/cm^3. The density difference is higher between water and bio rad leading to higher bouncy forces and lower velocity. To test this assumption, in the future, we will coat channels with a hydrophobic material, such as Teflon, and measure the velocity after the coating that should increase the velocity of the droplets. Additionally, it is noteworthy that with the increase of oil viscosity, the droplet size increases.

4.4.2 Droplet size

Several tests were carried out on different microfluidic devices, in order to analyze the effect of flow rates in droplet size and the device reliability.
In Fig: 4.18, three distinct flow behaviors were observed at different oil and water flow rates. When oil flow rate is significantly higher than water flow rate (represented by blue area), a stable interface between water and oil is formed and there is no droplet formation. In the case where oil flow rate is slightly smaller than water flow rate, "slugs" are formed instead of droplets (represented by green area). The "slugs" were detected by the comparison of major and minor axis length measures through Bonsai analysis. The major and minor axis are related to the maximum and minimum droplet diameter measured found by Bonsai. For spherical droplets, the ratio between the axis was ≈ 1 which results in equal droplet diameters along axis. Contrarily, ratios above 1 implies that the diameter measured for one axis is higher then the other, leading to "slugs".

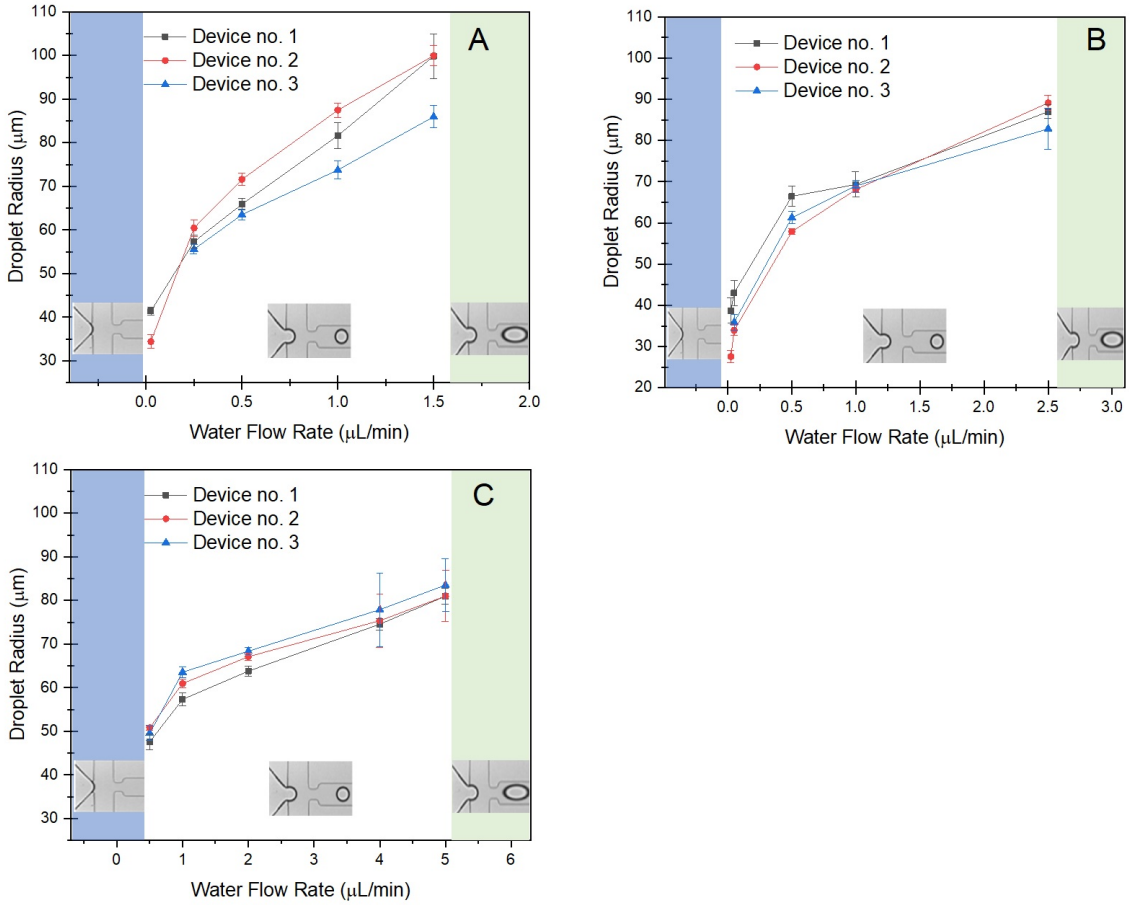

Figure 4.18: Experimental graph demonstrating the differences between the radius of the droplets produced by three different microfluidic devices: A) Oil flow rate of 1.25 μL/min; B) Oil flow rate of 2.5 μL/min; C) Oil Flow rate of 5 μL/min. The representations of droplet regimes were adapted from [44]

Thus, the droplet generation regime is situated between the two regimes described above. The results demonstrated in Fig: 4.18, show that the devices had similar results for the various tests, and maintained the same trend of increasing the radius of the droplet with the increase of water flow rate, and decreasing the radius with the increase of oil flows. Table: 4.1 depicts the droplet size variation between the boundary conditions for droplet regime. It is possible to observe that both flow rates has approximately the same influence regarding droplet size.

Table 4.1: Variation in droplet radius for different oil and water flow rates.

Oil Flow Rate / *Water Flow Rate*	*1.25 µL/min*	*5 µL/min*	*Relative Radius Variation*
0.5 µL/min	*71.58 µm*	*49.55 µm*	*- 31 %*
1.5 µL/min	*99.95 µm*	*64.78 µm*	*- 35 %*
Relative Radius Variation	*+ 40 %*	*+ 31 %*	

Regarding droplet size variations observed between devices, the differences can be explained by camera resolution. Due to this, during the calibration of pixels to micrometers, 1 pixel ranged between 8-12 μm. Besides, device no. 2 did not have the light setup optimized for droplet contour at Bonsai analysis. Thus, the calculation of droplet diameter for this device may not take into account the actual size of the droplet (Annex: III). Generally, process variability, both in device fabrication and during experimental tests, also contributed to the verified differences.

As a result of performed tests, the droplet generator presented in this work allowed to obtain droplets with a radius between approximately 27-99 μm. In order to evaluate droplet size dispersion, the Coefficient of Variation (CV) was calculated for each experimental condition. CV is a statistical measure of relative dispersion of data point in a data series around the mean, given by the follow equation:

$$CV(\%) = \frac{Standard\,Deviation}{Mean} \times 100 \tag{4.1}$$

The droplet size CV ranged between 1-10%, where 1% was achieved for oil flow rate at 1.25 μL/min and water flow rate 1 μL/min while 10% was achieved for oil flow rate at 5 μL/min and water flow rate 1 μL/min. Some reports obtained CV$<$ 5 %, for flow-focusing geometry [45, 46]. Once droplet radius was characterized, the droplet volumes were calculated (Figure: 4.19).

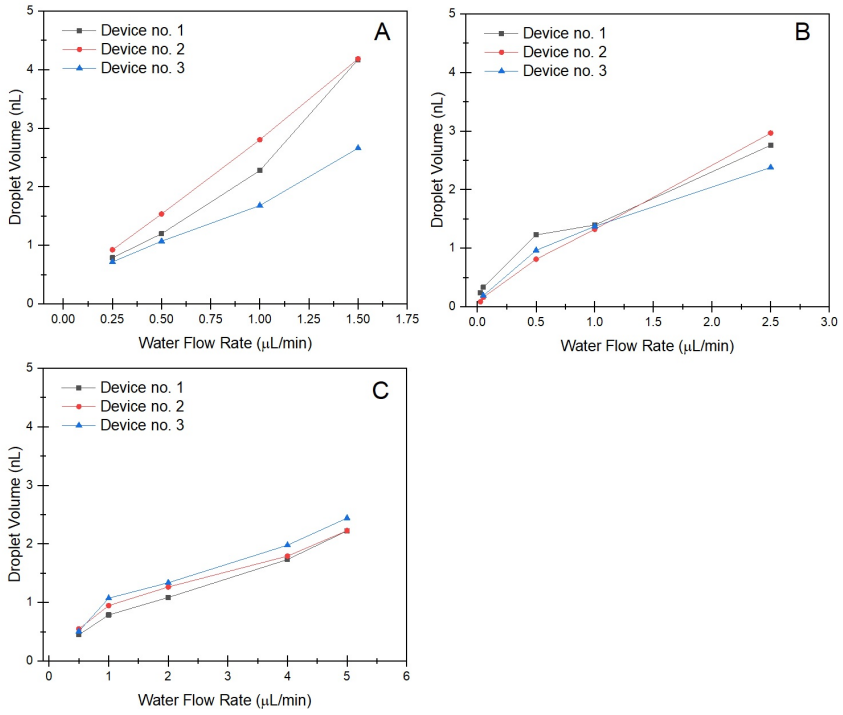

Figure 4.19: Experimental graph demonstrating the droplet volume produced by three different microdluidic devices, obtained through droplet sizes: A) Oil flow rate of 1.25 μL/min; B) Oil flow rate of 2.5 μL/min; C) Oil Flow rate of 5 μL/min.

Due to surface tensions, droplets tend to acquire the shape of spheres. Thus, the volume calculation was based on this condition. As a result, the droplet volumes obtained ranged from 90 pL-4.18 nL, which are adequate volumes for dPCR.

4.4.3 Droplet Velocity

The results about droplet velocity are demonstrated in Figure: 4.20.

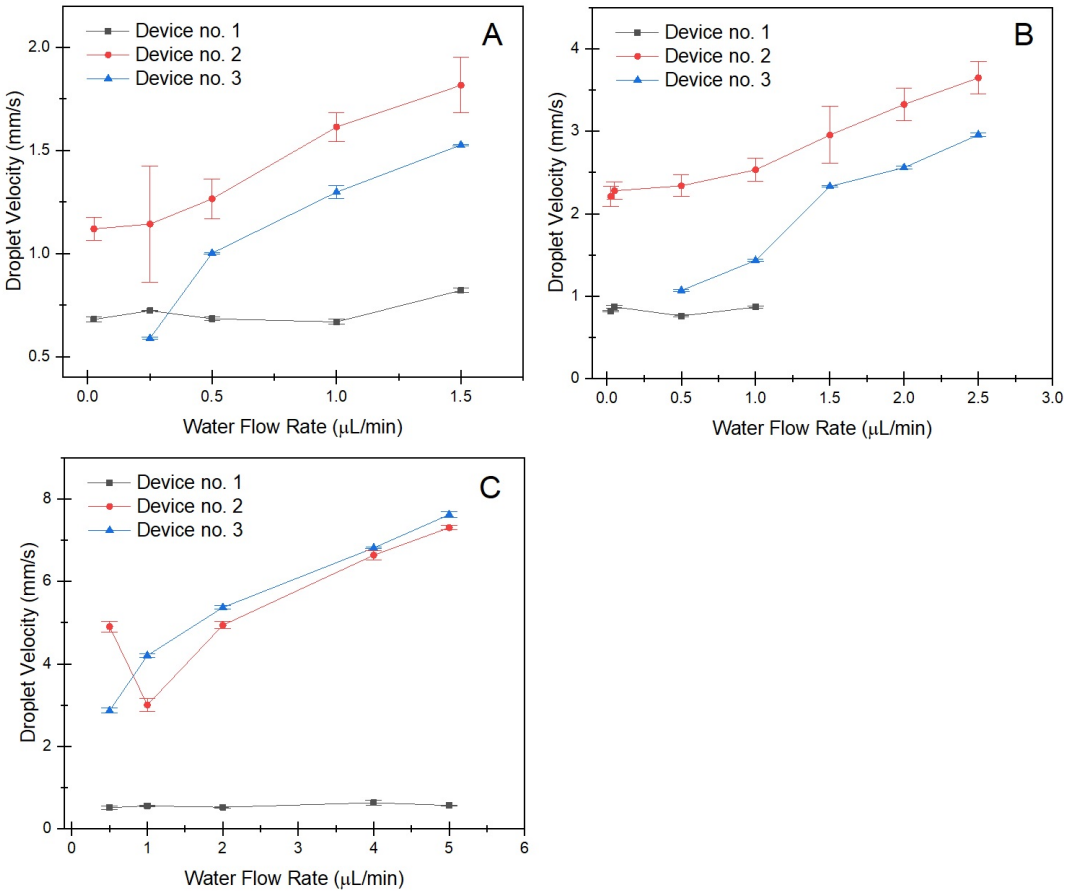

Figure 4.20: Experimental graph demonstrating the differences between the radius of the droplets produced by three different microfluidic devices: A) Oil flow rate of 1.25 μL/min; B) Oil flow rate of 2.5 μL/min; C) Oil Flow rate of 5 μL/min.

Droplet velocity is sensitive to environmental vibrations, being one of the reasons for the differences noticed. Additionally, devices no. 2 and no. 3 were fabricated using different master moulds (albeit with the same design) which can lead to slight variations on channels dimensions, more relevant in cases where the flow rates are low - low velocity - and for droplets with diameter approximated to the channel width. By the use of hydrophobic coating treatment in channels they can be made them to exhibit more hydrophobic proprieties, thus reducing overall friction and improving droplet mobility.
Regarding device no. 1, the noticeably lower velocity gave the first indication that the device may have had its oil channels corrupted. This hints that there is the possibility

of not enough oil flow rate reaching the junction. To find out if the cause was related to flaws in the device, dye diluted in water was placed in a syringe and the solution was injected into the oil inlet. It was possible to verify the existence of a connection between the oil inlet and the outlet on the device derived from an inefficient sealing (Annex: IV). Table 4.2 depicts the relative velocity variation between the boundary conditions for droplet regime. It is noteworthy that, with the increase of oil flow rate, the velocity of the droplets increases significantly when compared with the increase of water flow rate, which indicated the greater influence of continuous phase on droplet velocity.
With this droplet generator it was possible to obtain droplets with velocities ranging between 0.05 mm/s - 7.62 mm/s.

Table 4.2: Variation in droplet velocity for different oil and water flow rates conditions

Oil Flow Rate / *Water Flow Rate*	*1.25 µL/min*	*5 µL/min*	*Relative Velocity Variation*
0.5 µL/min	*1.00 mm/s*	*2.86 mm/s*	*+ 186 %*
1.5 µL/min	*1.52 mm/s*	*4.65 mm/s*	*+ 206 %*
Relative Velocity Variation	*+ 52 %*	*+ 63 %*	

4.4.4 Droplet Frequency

The figure 4.21 depicts the effect of the frequency of generating droplets for different flow rates of water and oil flows.

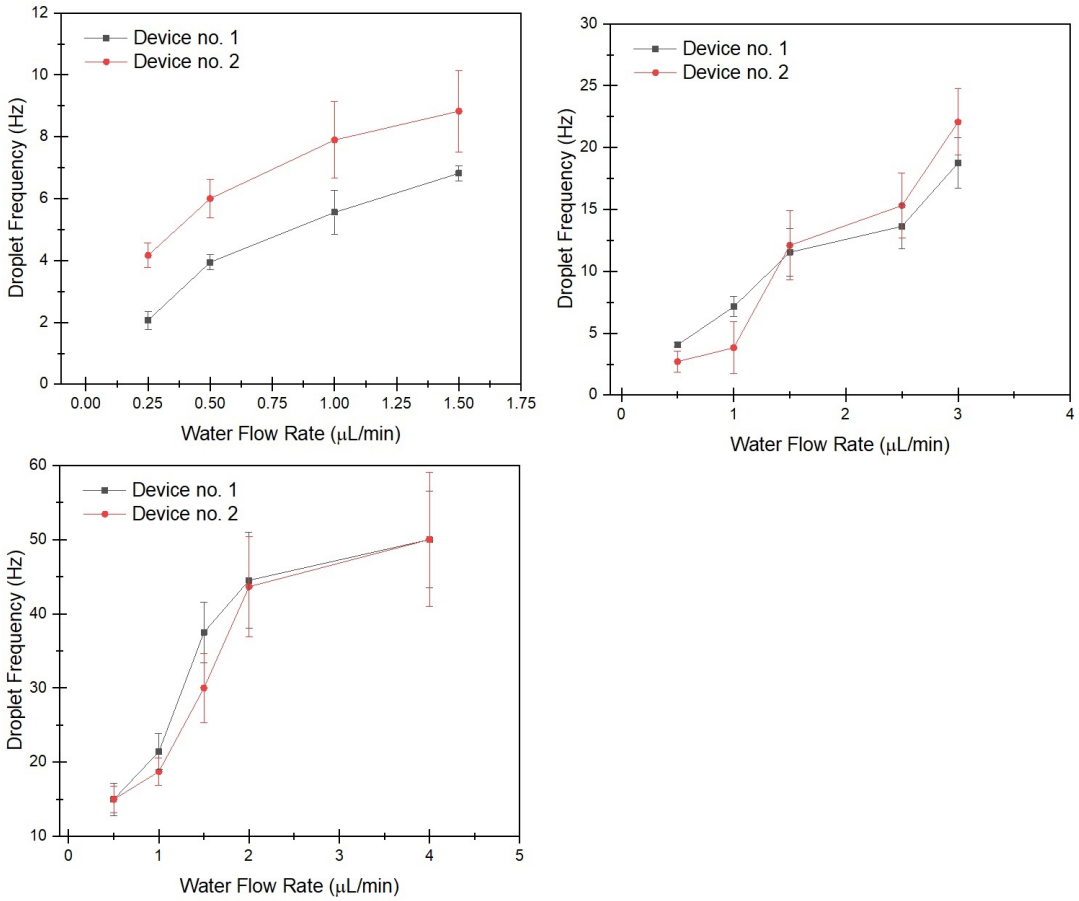

Figure 4.21: Experimental graph demonstrating the droplet generation frequency produced by two different microfluidic devices: A) Oil flow rate of 1.25 μL/min; B) Oil flow rate of 2.5 μL/min; C) Oil Flow rate of 5 μL/min.

Since device no. 3 was malfunctioning, it was not considered for these tests.
The results show that it was possible to obtain frequencies ranging from approximately 2-50 Hz. As the water and oil flow rates increase, the frequency of droplet generation also increases.

4.5 Serpentine Design

Once the droplet generator was optimized and droplet size, velocity and frequency characterized, serpentine design was incorporated for droplet-based continuous flow PCR (Figure: 4.22).
This design was made considering the reported serpentine designs in several articles for performing PCR in continuous flow.

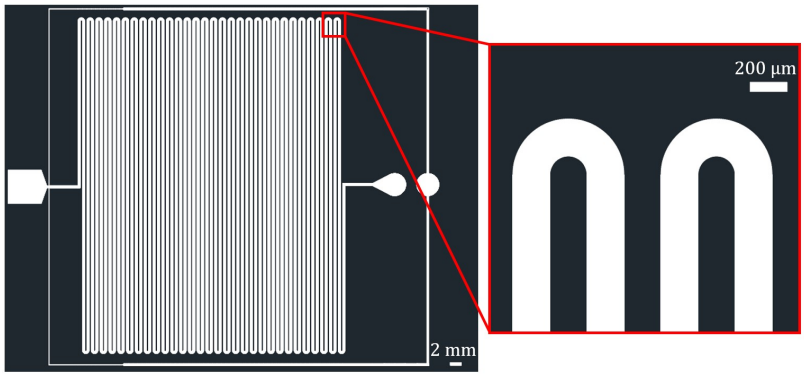

Figure 4.22: Serpentine with droplet generator design incorporated layout

The total channel length was 185 cm for performing 30 cycles of PCR, resulting in a total device footprint of 3.8 cm × 3.2 cm. The overall device dimension was limited by the holder existing in digital microfluidics that is part of the project in which this master thesis is inserted.
Regarding serpentine channels, its dimensions are 200 μm of width spaced by 200 μm.

4.5.1 Device Characterization

Regarding hard-mask characterization, the results revealed a great proximity between its dimensions and the design's dimensions resulting in an error of approximately 0.5%. Relatively to the dimensions of the device, there was a reduction in channel height by almost 10 μm due to the same reasons explained in section 4.1.3.2.

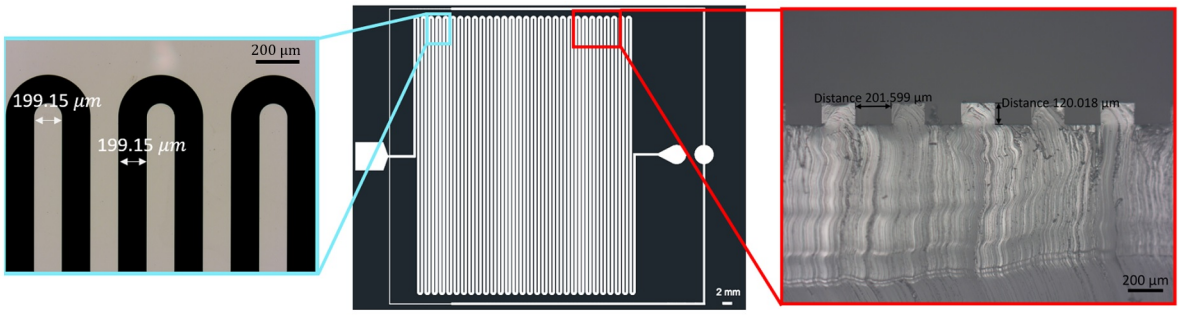

Figure 4.23: Serpentine with droplet generator design characterization: Hard mask dimensions (Left); Serpentine design layout (Center); Serpentine channel cross-section dimensions (Right)

4.5.2 Heating Tests and Droplet Characterization

The standard PCR thermal profile is often constituted by three thermal steps regarding denaturation, annealing and extension phases. However, annealing and extension temperatures can be merged, resulting in two temperature regions which denaturation phase is carry out at 95º C and the annealing and extension phase can undergo to temperatures between 65º C and 72º C.
Taking into account the device presented in this work, its geometry does not allow that all phases of the PCR cycle can be done with similar residence time for three temperature regions, since it will result in an extension region with approximately half of the length when compared to denaturation and annealing regions (Figure: 4.24).
For that, three ceramic resistors (2.3 cm × 1 cm) controlled by PID digital controllers will be used to heat the device through the Joule effect.

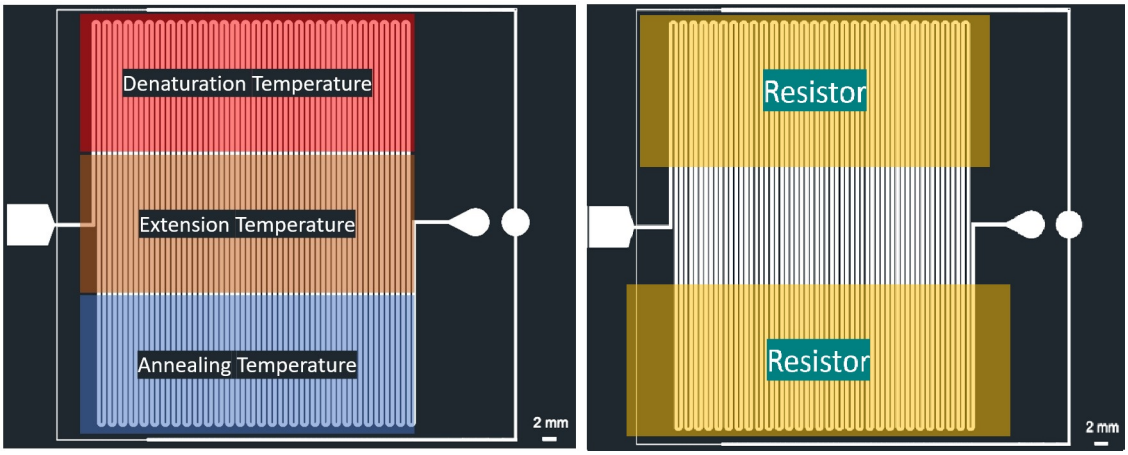

Figure 4.24: Schematic representation of temperature regions for PCR cycles, applied to the droplet-based continuous flow device (left) and representation of resistors application (right).

Due to the high influence of flow rates in droplet velocity, and thus in droplet residence time, their determination is crucial to guarantee an adequate droplet velocity.
According to geometry restrictions mentioned, the total time considered for PCR process was 45 min, corresponding to 30 s at denaturation phase, 30 s at extension phase, and 30 s at annealing phase. For the purpose of initial tests for analysing droplet behaviour with temperature, the heating and cooling times of the resistors were not considered. Taking these times into account, as well as the cycle length, the flow rate necessary to guarantee an adequate droplet velocity can be calculated through:

$$Q = v \times A = \frac{d}{t} \times A \quad \left(\frac{\mu m^3}{min}\right) \tag{4.2}$$

where Q is the total flow rate, A is the channel cross-sectional area, v is the average velocity, d is the total distance and t is the total time.

From equation 4.2 the total flow rate that allows a droplet velocity of approximately 0.68 mm/s is 1.07 μL/min. As discussed before, the oil flow rate has a greater influence in droplet velocity, thus, this flow rate calculated was relatively to oil, while water flow rate can be adjusted concerning the ratios that allows droplet generation regime.
Given the crucially of the droplet velocity, Bonsai will allow adjusting, in real-time, the flow rates according to the necessary velocity for the PCR cycles, thus working in a closed-loop with the flow controllers.
Considering the previous studies done in this work for droplet characterization, at this flow rate it is expected to have droplets with sizes below 55-60 μm with frequencies ranging between 3-5 Hz. Additionally, due to the inherent complexity of serpentine design, the droplets are expected to travel at lower velocity when compared to the velocities obtained in this study.

Chapter Five

Conclusions and Future Perspectives

This master thesis work was intended to develop and optimize a high-throughput droplet-based microfluidic device for application in dPCR with a real-time analysis software for droplet monitoring.

The results of device characterization revealed that the fabrication process is robust, leading to device reproducibility.

With the objective to monitor the droplets in real time, Bonsai was chosen as the video analysis software, as opposed to other more widely used alternatives, due to its capability to interpret and cross-analyze various parallel data streams in real time. Moreover, Bonsai has the ability to be used as a controller allowing for a self-correcting closed-loop to be employed.

Droplet size and velocity were characterized through Bonsai, which results matched well with the results obtained through Image J. Regarding droplet frequency, the results were compared with those extracted from video observation and revealed approximation between them. In this way, we envision that the developed Bonsai workflow will be a powerful tool for real-time droplet monitoring.

Regarding droplet volumes it was possible to obtain volumes between 90 pL-4.18 nL that are suitable for a high-throughput dPCR technique. Moreover, it was possible to obtain low droplet velocities for dPCR thermal cycles.

With the droplet generator device optimized, and the serpentine design incorporated into it, it is now applicable for PCR test cycles in continuous flow.

In the future, temperature tests need to be performed in order to understand its distribution along the device as well as the droplet behaviour with temperature. Additionally, serpentine design must be adapted according to the thermal cycle specifications.

Furthermore, Bonsai can also be used for dPCR detection through label-free monitoring.

Bibliography

[1] *WHO | Key statistics*. URL: https://www.who.int/cancer/resources/keyfacts/en/ (visited on 12/12/2020).

[2] M. Plummer, C. de Martel, J. Vignat, J. Ferlay, F. Bray, and S. Franceschi. "Global burden of cancers attributable to infections in 2012: a synthetic analysis." In: *The Lancet Global Health* 4.9 (2016), e609–e616. ISSN: 2214109X. DOI: 10.1016/S2214-109X(16)30143-7.

[3] D. W. Cescon, S. V. Bratman, S. M. Chan, and L. L. Siu. "Circulating tumor DNA and liquid biopsy in oncology." In: *Nature Cancer* 1.3 (2020), pp. 276–290. ISSN: 2662-1347. DOI: 10.1038/s43018-020-0043-5. URL: http://dx.doi.org/10.1038/s43018-020-0043-5.

[4] C. Fiala and E. P. Diamandis. *Utility of circulating tumor DNA in cancer diagnostics with emphasis on early detection*. 2018. DOI: 10.1186/s12916-018-1157-9. URL: https://bmcmedicine.biomedcentral.com/articles/10.1186/s12916-018-1157-9.

[5] *What is circulating tumor DNA and how is it used to diagnose and manage cancer?: MedlinePlus Genetics*. URL: https://medlineplus.gov/genetics/understanding/testing/circulatingtumordna/ (visited on 12/11/2020).

[6] M. Elazezy and S. A. Joosse. *Techniques of using circulating tumor DNA as a liquid biopsy component in cancer management*. 2018. DOI: 10.1016/j.csbj.2018.10.002. URL: /pmc/articles/PMC6197739/?report=abstracthttps://www.ncbi.nlm.nih.gov/pmc/articles/PMC6197739/.

[7] *Polymerase Chain Reaction on JSTOR*. URL: https://www.jstor.org/stable/30137034?seq=1 (visited on 12/03/2020).

[8] *Microfluidic PCR & qPCR - Elveflow*. URL: https://www.elveflow.com/microfluidic-reviews/general-microfluidics/microfluidic-pcr-qpcr-rtpcr/ (visited on 12/03/2020).

[9] *What is PCR? — Science Learning Hub*. URL: https://www.sciencelearn.org.nz/resources/2347-what-is-pcr (visited on 12/03/2020).

[10] H. A. Erlich. "Polymerase chain reaction." In: *Journal of Clinical Immunology* 9.6 (1989), pp. 437–447. ISSN: 02719142. DOI: 10.1007/BF00918012.

[11] L. Garibyan and N. Avashia. "research Techniques made simple Polymerase Chain Reaction." In: *Journal of Investigative Dermatology* 133 (2013), p. 6. DOI: 10.1038/jid.2013.1. URL: www.jidonline.org.

[12] *Digital PCR | Thermo Fisher Scientific - PT*. URL: https://www.thermofisher.com/pt/en/home/life-science/pcr/digital-pcr.html (visited on 12/04/2020).

[13] P. L. Quan, M. Sauzade, and E. Brouzes. *DPCR: A technology review*. 2018. DOI: 10.3390/s18041271. URL: /pmc/articles/PMC5948698/?report=abstracthttps://www.ncbi.nlm.nih.gov/pmc/articles/PMC5948698/.

[14] "Beaming and droplet digital pcr analysis of mutant idh1 mrna in glioma patient serum and cerebrospinal fluid extracellular vesicles." In: *Molecular Therapy - Nucleic Acids* 2 (2013), e109.

[15] *Digital PCR - QIAGEN*. URL: https://www.qiagen.com/us/applications/digital-pcr (visited on 12/12/2020).

[16] L. Cao, X. Cui, J. Hu, Z. Li, J. R. Choi, Q. Yang, M. Lin, L. Ying Hui, and F. Xu. "Advances in digital polymerase chain reaction (dPCR) and its emerging biomedical applications." In: *Biosensors and Bioelectronics* 90 (2017), pp. 459–474. ISSN: 18734235. DOI: 10.1016/j.bios.2016.09.082. URL: http://dx.doi.org/10.1016/j.bios.2016.09.082.

[17] G. Perkins, H. Lu, F. Garlan, and V. Taly. "Droplet-Based Digital PCR: Application in Cancer Research." In: *Advances in Clinical Chemistry* 79 (2017), pp. 43–91. ISSN: 00652423. DOI: 10.1016/bs.acc.2016.10.001.

[18] K. Kant and S. Abalde-Cela. *Surface-enhanced raman scattering spectroscopy and microfluidics: Towards ultrasensitive label-free sensing*. 2018. DOI: 10.3390/bios8030062. URL: http://www.mdpi.com/2079-6374/8/3/62.

[19] A. B. Theberge, F. Courtois, Y. Schaerli, M. Fischlechner, C. Abell, F. Hollfelder, and W. T. Huck. *Microdroplets in microfluidics: An evolving platform for discoveries in chemistry and biology*. 2010. DOI: 10.1002/anie.200906653. URL: https://onlinelibrary.wiley.com/doi/full/10.1002/anie.200906653https://onlinelibrary.wiley.com/doi/abs/10.1002/anie.200906653https://onlinelibrary.wiley.com/doi/10.1002/anie.200906653.

[20] H. Jayamohan, V. Romanov, H. Li, J. Son, R. Samuel, J. Nelson, and B. K. Gale. "Advances in Microfluidics and Lab-on-a-Chip Technologies." In: *Molecular Diagnostics: Third Edition*. Elsevier Inc., 2017, pp. 197–217. ISBN: 9780123745378. DOI: 10.1016/B978-0-12-802971-8.00011-0. URL: https://linkinghub.elsevier.com/retrieve/pii/B9780128029718000110.

[21] C. Zhang and D. Xing. "Miniaturized PCR chips for nucleic acid amplification and analysis: Latest advances and future trends." In: *Nucleic Acids Research* 35.13 (2007), pp. 4223–4237. ISSN: 03051048. DOI: 10.1093/nar/gkm389.

[22] I. Wong and C. M. Ho. "Surface molecular property modifications for poly(dimethylsiloxane) (PDMS) based microfluidic devices." In: *Microfluidics and Nanofluidics* 7.3 (2009), pp. 291–306. ISSN: 16134982. DOI: 10.1007/s10404-009-0443-4.

[23] S. Mohr, Y. H. Zhang, A. Macaskill, P. J. Day, R. W. Barber, N. J. Goddard, D. R. Emerson, and P. R. Fielden. "Numerical and experimental study of a droplet-based PCR chip." In: *Microfluidics and Nanofluidics* 3.5 (2007), pp. 611–621. ISSN: 16134982. DOI: 10.1007/s10404-007-0153-8.

[24] T. S. Kaminski, O. Scheler, and P. Garstecki. "Droplet microfluidics for microbiology: Techniques, applications and challenges." In: *Lab on a Chip* 16.12 (2016), pp. 2168–2187. ISSN: 14730189. DOI: 10.1039/c6lc00367b.

[25] C. N. Baroud, F. Gallaire, and R. Dangla. *Dynamics of microfluidic droplets*. 2010. DOI: 10.1039/c001191f. URL: http://xlink.rsc.org/?DOI=c001191f.

[26] T. P. Lagus and J. F. Edd. "High-throughput co-encapsulation of self-ordered cell trains: Cell pair interactions in microdroplets." In: *RSC Advances* 3.43 (2013), pp. 20512–20522. ISSN: 20462069. DOI: 10.1039/c3ra43624a. URL: www.rsc.org/advances.

[27] S. Y. Teh, R. Lin, L. H. Hung, and A. P. Lee. *Droplet microfluidics*. 2008. DOI: 10.1039/b715524g. URL: http://xlink.rsc.org/?DOI=b715524g.

[28] *(PDF) In vivo and in vitro directed evolution of enzymes using droplet-based microfluidics*. URL: https://www.researchgate.net/publication/278826711{_}In{_}vivo{_}and{_}in{_}vitro{_}directed{_}evolution{_}of{_}enzymes{_}using{_}droplet-based{_}microfluidics (visited on 12/09/2020).

[29] W. Lee, L. M. Walker, and S. L. Anna. "Role of geometry and fluid properties in droplet and thread formation processes in planar flow focusing." In: *Physics of Fluids* 21.3 (2009), p. 032103. ISSN: 10706631. DOI: 10.1063/1.3081407. URL: http://aip.scitation.org/doi/10.1063/1.3081407.

[30] T. Ward, M. Faivre, M. Abkarian, and H. A. Stone. "Microfluidic flow focusing: Drop size and scaling in pressure versus flow-rate-driven pumping." In: *Electrophoresis* 26.19 (2005), pp. 3716–3724. ISSN: 01730835. DOI: 10.1002/elps.200500173. URL: http://doi.wiley.com/10.1002/elps.200500173.

[31] J. C. Baret. *Surfactants in droplet-based microfluidics*. 2012. DOI: 10.1039/c1lc20582j.

[32] C. Frey, J. Pfeil, T. Neckernuss, D. Geiger, K. Weishaupt, I. Platzman, O. Marti, and J. P. Spatz. "Label-free monitoring and manipulation of microfluidic water-in-oil droplets." In: *View* 1.4 (2020), p. 20200101. ISSN: 2688-268X. DOI: 10.1002/viw.20200101. URL: https://onlinelibrary.wiley.com/doi/full/10.1002/VIW.20200101https://onlinelibrary.wiley.com/doi/abs/10.1002/VIW.20200101https://onlinelibrary.wiley.com/doi/10.1002/VIW.20200101.

[33] A. S. Basu. "Droplet morphometry and velocimetry (DMV): A video processing software for time-resolved, label-free tracking of droplet parameters." In: *Lab on a Chip* 13.10 (2013), pp. 1892–1901. ISSN: 14730189. DOI: 10.1039/c3lc50074h. URL: https://pubs.rsc.org/en/content/articlehtml/2013/lc/c3lc50074hhttps://pubs.rsc.org/en/content/articlelanding/2013/lc/c3lc50074h.

[34] E. W. Kemna, L. I. Segerink, F. Wolbers, I. Vermes, and A. Van Den Berg. "Label-free, high-throughput, electrical detection of cells in droplets." In: *Analyst* 138.16 (2013), pp. 4585–4592. ISSN: 13645528. DOI: 10.1039/c3an00569k. URL: https://pubs.rsc.org/en/content/articlehtml/2013/an/c3an00569khttps://pubs.rsc.org/en/content/articlelanding/2013/an/c3an00569k.

[35] C. Song, T. Jin, R. Yan, W. Qi, T. Huang, H. Ding, S. H. Tan, N. T. Nguyen, and L. Xi. "Opto-acousto-fluidic microscopy for three-dimensional label-free detection of droplets and cells in microchannels." In: *Lab on a Chip* 18.9 (2018), pp. 1292–1297. ISSN: 14730189. DOI: 10.1039/c8lc00106e. URL: https://pubmed.ncbi.nlm.nih.gov/29619468/.

[36] G. Lopes, N. Bonacchi, J. Frazão, J. P. Neto, B. V. Atallah, S. Soares, L. Moreira, S. Matias, P. M. Itskov, P. A. Correia, R. E. Medina, L. Calcaterra, E. Dreosti, J. J. Paton, and A. R. Kampff. "Bonsai: An event-based framework for processing and controlling data streams." In: *Frontiers in Neuroinformatics* 9.APR (2015). ISSN: 16625196. DOI: 10.3389/fninf.2015.00007.

[37] *Operators - Bonsai*. URL: https://bonsai-rx.org/docs/operators/ (visited on 12/11/2020).

[38] H. Gu, M. H. Duits, and F. Mugele. "A hybrid microfluidic chip with electrowetting functionality using ultraviolet (UV)-curable polymer." In: *Lab on a Chip* 10.12 (2010), pp. 1550–1556. ISSN: 14730189. DOI: 10.1039/c001524e.

[39] M. Mastiani, S. Seo, B. Mosavati, and M. Kim. "High-Throughput Aqueous Two-Phase System Droplet Generation by Oil-Free Passive Microfluidics." In: *ACS Omega* 3.8 (2018), pp. 9296–9302. ISSN: 24701343. DOI: 10.1021/acsomega.8b01768.

[40] *wrMTrck multible object tracker*. URL: http://www.phage.dk/plugins/wrmtrck.html (visited on 12/11/2020).

[41] F. Lapierre, N. Wu, and Y. Zhu. "Influence of flow rate on the droplet generation process in a microfluidic chip." In: (2011). DOI: 10.1117/12.903271. URL: http://spiedl.org/terms.

[42] K. Loizou, V.-L. Wong, and B. Hewakandamby. "Examining the Effect of Flow Rate Ratio on Droplet Generation and Regime Transition in a Microfluidic T-Junction at Constant Capillary Numbers." In: *Inventions* 3.3 (2018), p. 54. ISSN: 2411-5134. DOI: 10.3390/inventions3030054. URL: http://www.mdpi.com/2411-5134/3/3/54.

[43] *Droplet Digital™ PCR (ddPCR™) Technology | LSR | Bio-Rad*. URL: https://www.bio-rad.com/en-pt/applications-technologies/droplet-digital-pcr-ddpcr-technology?ID=MDV31M4VY (visited on 12/12/2020).

[44] A. J. T. Teo, K.-h. H. Li, N.-t. Nguyen, W. Guo, N. Heere, H.-d. Xi, C.-w. Tsao, W. Li, and S. H. Tan. "Negative Pressure Induced Droplet Generation in a Micro fl uidic Flow-Focusing Device." In: (2017). DOI: 10.1021/acs.analchem.6b05053.

[45] P. Zhu and L. Wang. "Passive and active droplet generation with microfluidics: a review." In: *Lab on a Chip* 17.1 (2017), pp. 34–75. ISSN: 14730189. DOI: 10.1039/C6LC01018K. URL: http://dx.doi.org/10.1039/C6LC01018K.

[46] R. H. Baughman et al. "An Axisymmetric Flow-Focusing Microfluidic Device**." In: *Compos. Sci. Technol* 62 (2002), p. 29. DOI: 10.1002/adma.200401738. URL: http://www.advmat.de.

Annex One

Annex 1

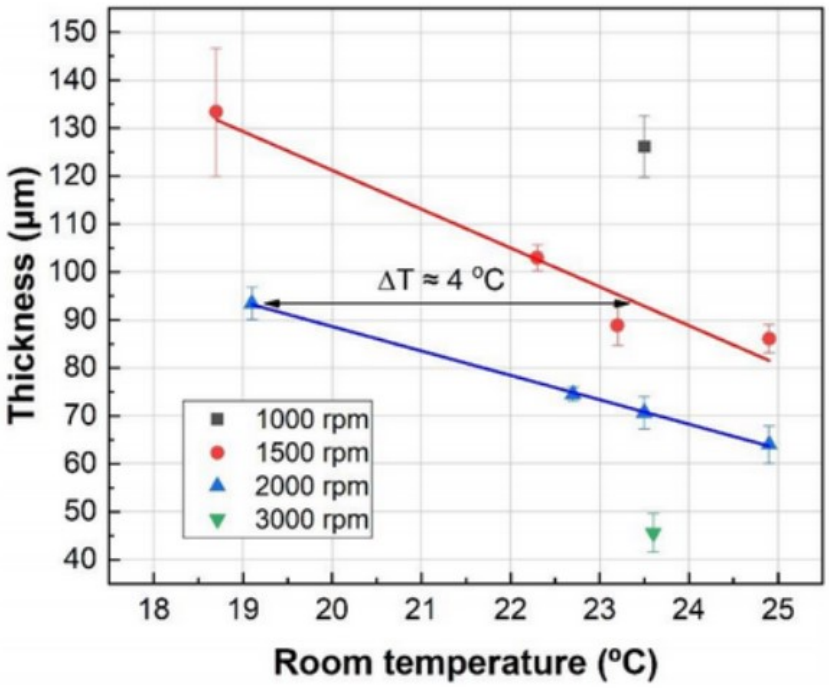

Figure I.1: Experimental calibrations depicting the variation of SU-8 thickness with room temperature and with different spin-coating parameters.

Annex Two

Annex 2

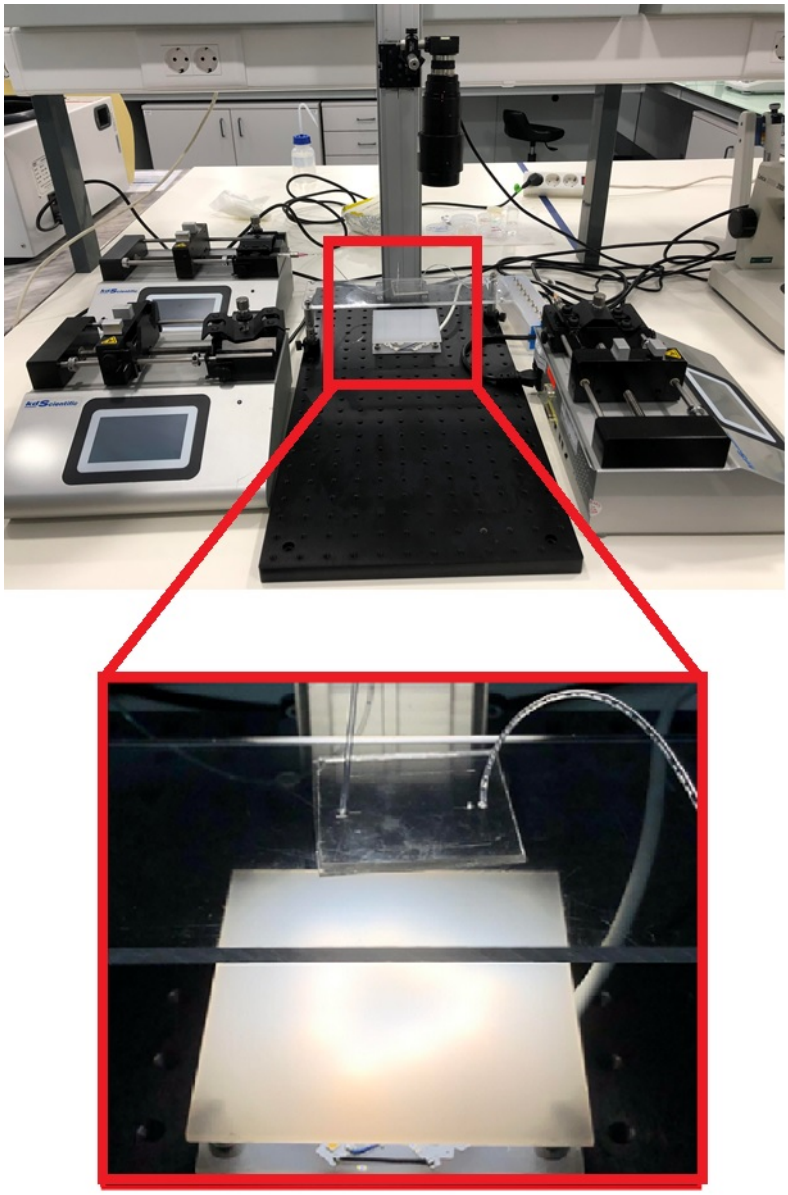

Figure II.1: Setup used for droplet characterization

Annex Three

Annex 3

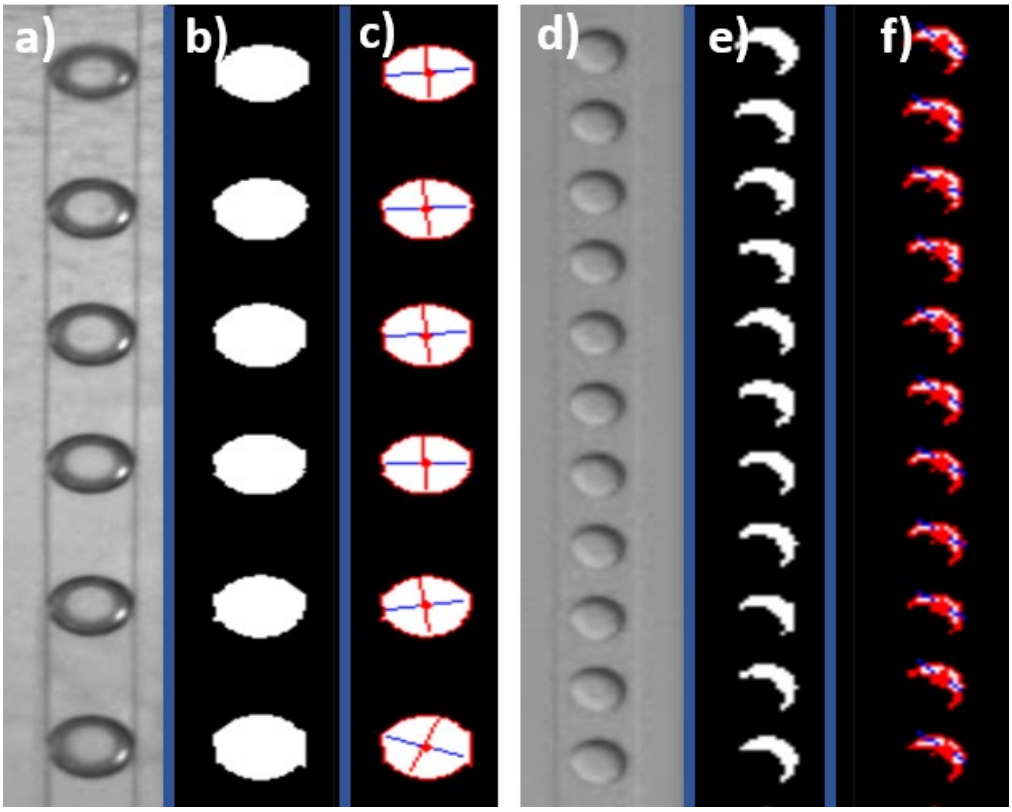

Figure III.1: Differences at Bonsai analysis for different light conditions: a), d): Delimitated ROI; b), e) Droplet countours defined by FindCountours node ; c), f) Diameters considered by the *Binary Region Analysis* node.

Annex Four

Annex 4

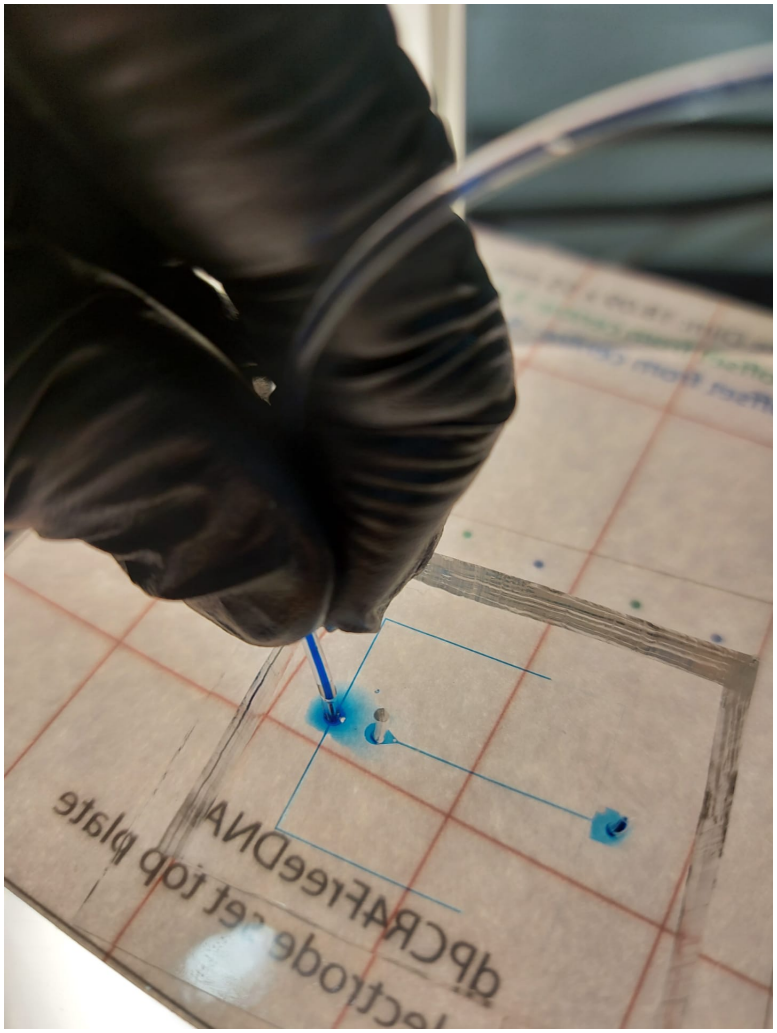

Figure IV.1: Connection between oil inlet and outlet verified in device no. 1 through dye injection.